A REVIEW OF DIODE AND SOLAR CELL EQUIVALENT CIRCUIT MODEL LUMPED PARAMETER EXTRACTION PROCEDURES

Adelmo Ortiz-Conde, Francisco J. García-Sánchez, Juan Muci, Andrea Sucre-González

Solid State Electronics Laboratory, Simón Bolívar University, Caracas 1080A, Venezuela

Abstract. *This article presents an up-to-date review of several methods used for extraction of diode and solar cell model parameters. In order to facilitate the choice of the most appropriate method for the given particular application, the methods are classified according to their lumped parameter equivalent circuit model: single-exponential, double-exponential, multiple-exponential, with and without series and parallel resistances. In general, methods based on numerical integration or optimization are recommended to reduce the possible uncertainties arising from measurement noise.*

Key words: *solar cell, diode, single-exponential, double-exponential, multiple-exponential*

1. INTRODUCTION

Photovoltaic energy conversion has received great attention recently and much research has been dedicated to solar cells. Practical applications of solar cells require simple lumped models and efficient parameter extraction methods. Parameter extraction in solar cells has been a research topic for many years [1] and several articles [2]-[11] have reviewed over time the different parameter extraction methods in diodes and solar cells. Although last year Cotfas et al reviewed [2] 34 different methods, not all the methods were included.

The pioneering fabrication of the first silicon p-n junction and solar cell by Ohl in 1940 was presented in a patent in 1941 [12]. Ohl and his colleagues in Bell Labs were studying silicon as a detector and they were trying to obtain pure silicon by fusing silica (SiO_2) and slowly cooling the fused material until it solidified. As a result, impurities inside the silicon spontaneously segregated forming a p-n junction by serendipity [13], [14]. They observed that the device produced electrical energy when it received light. Shockley developed [15] the theory of p-n junctions in 1949, and presented the first

single-exponential model for a p-n junction with series resistance. Chapin et al published in 1954 the first article dedicated to the silicon photocell [16]. Prince published in 1955 the first single-exponential model for a solar cell with series and parallel resistance [17] and, considering that all the research so far was done from Bell Labs, he referred to the solar cell as the Bell Solar Battery [17]. Sah, Noyce and Shockley published in 1957 the first multi-exponential model for a p-n junction with series resistance [18].

In the following sections we will review available methods for parameter extraction in diodes and solar cells. We consider that the choice of the best method depends on each particular application, based on the appropriate lumped parameter equivalent circuit model to be used. An important consideration is measurement noise, which obscures parameter extraction, especially if the method is based on using few experimental points [19]-[21]. Two possible ways exist when measurement noise is high: (i) applying conventional data smoothing to reduce the possible uncertainties arising from measurement noise; and (ii) using a robust technique based on taking many points, as for example, numerical integration [22]-[24] or optimization [25], [26]. Another future promising solution, which is not going to be evaluated in the present article, consists in the use of genetic algorithms [27], [28].

In order to facilitate the choice of the most appropriate method for a given particular application, the different methods will be organized according to their corresponding lumped parameter equivalent circuit model. Section 2 reviews parameter extraction using the single-exponential diode model for three different cases: without any resistance, with series resistance, and with both series and parallel resistances. Section 3 presents parameter extraction using multiple-exponential diode models. Section 4 scrutinizes parameter extraction using the single-exponential solar cell model for the following cases: without any resistance, with series resistance, with parallel resistance, and with series and parallel resistances. Finally, Section 5 reviews and discusses parameter extraction using multiple-exponential solar cell models.

2. SINGLE-EXPONENTIAL DIODE MODEL

2.1. Single-exponential diode model without any resistance

Consider an idealized diode without resistance whose *I-V* characteristics may be described by a lumped parameter equivalent circuit model consisting of a single exponential-type ideal junction [15]. Figure 1 presents the equivalent circuit of such a model. The terminal current, *I*, of this lumped parameter equivalent circuit model is explicitly described in mathematical terms by Shockley's equation:

$$I = I_0 \left[\exp\left(\frac{V}{n v_{th}} \right) - 1 \right] \tag{1}$$

where *V* is the terminal voltage, I_0 is the reverse current, *n* is the so-called diode quality factor, and $v_{th} = k_B T/q$ is the thermal voltage. Alternatively the terminal voltage may be expressed as an explicit function of the terminal current:

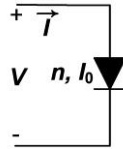$$V = n v_{th} \ln\left(1 + \frac{I}{I_0}\right).$$ (2)

Fig. 1 Idealized diode equivalent circuit without parasitic resistances

Figure 2 presents measurements of a silicon diode from Motorola [25] and simulated *I-V* characteristic of an idealized diode, in linear and logarithmic scales. Neglecting the -1 term in (1), which is equivalent to the assumption that $I \gg I_0$, yields:

(3)

$$\ln(I) = \ln(I_0) + \frac{V}{n v_{th}}.$$

Therefore, the plot of $\ln(I)$ vs V is a straight line whose slope, $1/n v_{th}$, and *V*-axis intercept yield at room temperature $n=1.03$ and $I_0=0.55$ nA, respectively.
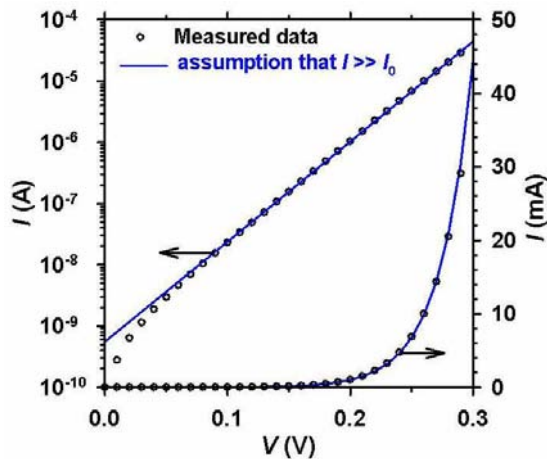

Fig. 2 Measurement (symbols) and simulation (lines) of a silicon diode *I-V* characteristics at room temperature in linear and logarithmic scales. Simulations are done using (3) which assumes $I \gg I_0$ and results in a straight line in logarithmic scale

2.2. Single-exponential diode model with series resistance

Figure 3 presents the lumped parameter equivalent circuit model of a diode with parasitic series resistance. As a consequence of the presence of the parasitic series resistance R_s, the terminal current of this equivalent circuit is mathematically described by an implicit equation:

$$I = I_0 \left[\exp\left(\frac{V - R_s I}{n v_{th}} \right) - 1 \right] . \tag{4}$$
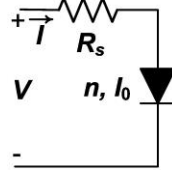

Fig. 3 Diode equivalent circuit with a parasitic series resistance

The terminal voltage can be mathematically solved from the previous equation as an explicit function of the terminal current:

$$V = R_s I + n v_{th} \ln\left(1 + \frac{I}{I_0} \right) . \tag{5}$$

The implicit terminal current equation given by (4) can be solved explicitly in terms of the terminal voltage if we introduce the use of the special *Lambert W* function [29], [30]:

$$I = \frac{n v_{th}}{R_s} W_0 \left\{ \frac{I_0 R_s}{n v_{th}} \exp\left[\frac{(V + I_0 R_s)}{n v_{th}} \right] \right\} - I_0 , \tag{6}$$

where W_0 represents the principal branch of the *Lambert W* function [31] which is a special function defined as the solution to the equation $W(x) \exp(W(x))=x$. The *Lambert W* function has already proved its usefulness in numerous physics applications [32], [33].

Figure 4 presents AIM-SPICE [34] simulations of a diode with several values of the series resistance. It is important to observe that the effect of Rs is significant for the high voltage region and that the region where ln(I) is proportional to V decreases as Rs increases.

2.2.1. *Vertical and lateral optimization methods*

The three parameters (n, I_0 and R_S) that fully describe the diode in terms of this lumped parameter equivalent circuit model can be extracted by fitting the cell's measured data to any of the model's defining equations. Equations (4), (5) or (6) can be applied directly for fitting. Vertical or lateral optimization could be used for fitting by minimizing either the voltage quadratic error or the current quadratic error, respectively. In the present case the use of equation (5) in combination with lateral optimization [25], [35] affords the best computational convenience, since this equation is not implicit, as (4) is, and does not contain special functions, as (6) does. Figure 5 presents measurements of a silicon diode from Motorola [25] and simulated *I-V* characteristic of a diode, in linear and logarithmic scales, using the parameters extracted by lateral optimization [25].
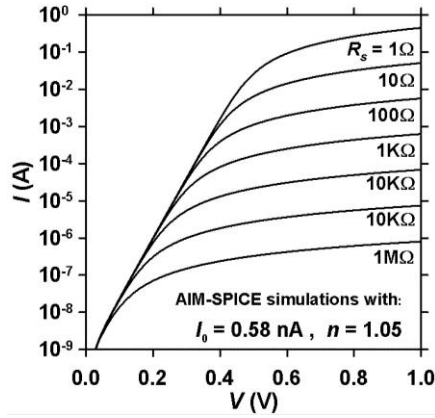
Fig. 4 AIM-SPICE simulations of a diode with several values of series resistance
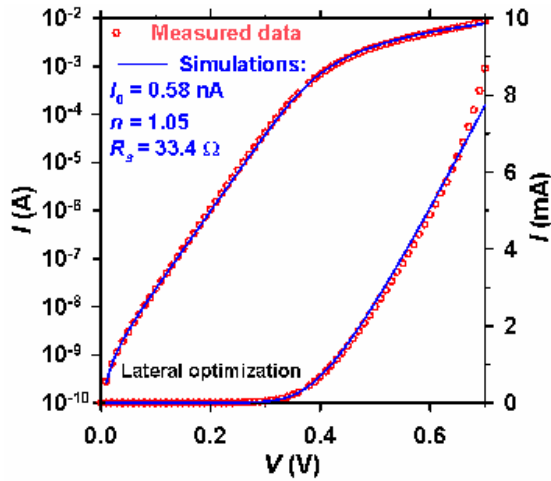

Fig. 5 Measured *I-V* characteristics of a silicon diode and its simulation
using the parameter values extracted by lateral optimization [25]

2.2.2. *Integration method to extract series resistance and ideality factor*

Following the idea of Araujo and Sánchez about the use of integration for parameter extraction [36], the drain current may be integrated by parts in combination with (5):

$$\int_0^V I \, dV = V \, I - \int_0^I V \, dI = \frac{R_s}{2} I^2 + n v_{th} \, I - I_0 \, V \quad . \tag{7}$$

Assuming that $I \gg I_0$ the last term in the above equation can be neglected and we obtain [37], [38]:

$$\int_0^V I \, dV \approx \frac{R_s}{2} I^2 + n v_{th} \, I \quad . \tag{8}$$

Therefore, a plot of the numerical integration of the measured current with respect to voltage is represented by an explicit algebraic quadratic function of I, which requires a much simpler fitting procedure than the original implicit equation. Kaminski et al later generalized this method [39] by allowing an arbitrary lower integration limit (V_i, I_i) instead of the origin, so that (8) becomes:

$$\frac{1}{I-I_i}\int_{V_i}^{V} I\, dV \approx \frac{R_s}{2}\left(I+I_i\right)+n v_{th}.$$ (9)

2.2.3. *The integral difference function concept and the G method*

We proposed a different approach [22], [23] that does not start with the extraction of the parasitic series resistance value. Instead, it does just the opposite. The proposed method is based on calculating an auxiliary function, or rather an operator, whose purpose is to eliminate the effect of the parasitic series resistance, retaining only the intrinsic model parameters. This new function was originally called "Integral Difference Function," it is denoted "Function D," and is defined as:

$$D(V,I) \equiv \int_0^I V\, dI - \int_0^V I\, dV = IV - 2\int_0^V I\, dV = 2\int_0^I V\, dI - IV \quad,$$ (10)

where D has units of "power." The integrals with respect to I and V are the device's "*Content*" and "*Co-content*", respectively, as shown in Fig. 6. For simplicity's sake and without loss of generality, the lower limit of integration in (10) is taken at the origin, but it may equally be placed at any arbitrary point of interest along the device's characteristics. Notice that adding the *Content* and *Co-content*, instead of subtracting them, as in (10), yields the device's total power.

It can be proved that in any given lumped parameter equivalent circuit model only nonlinear branches produce non-zero terms, and thus they are the only elements that contribute to the total D seen at the terminals. This property embodies the essence of the function D's ability to eliminate parasitic resistances (linear elements) from device models.
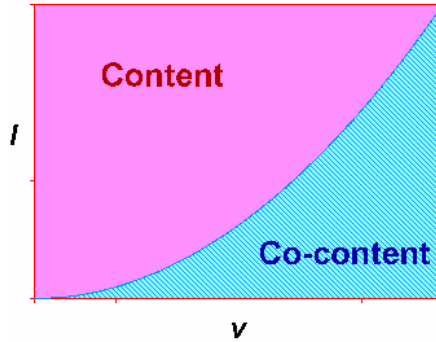

Fig. 6 Schematic illustration of the Content (C) and Co-Content (CC)
of a simple case of nonlinear function

It is important to point out that function D may be understood as a representation or measure of the device's amount of nonlinearity, which for a linear element is obviously equal to zero. This description of function D, in terms of linearity, led us to refer to this function as the "Integral Non Linearity Function" (*INLF*) [40], [41], and to use it to quantify the non-linear behavior of devices and circuits in terms of distortion.

Applying function D to the case of a single-exponential diode model with series resistance and restricting the analysis to the region of the measured forward characteristics, where $I \gg I_0$, the substitution of (5) into (10) yields [22], [23]:

$$D \approx I\,n\,v_{th}\left[\ln(I/I_0) - 2\right] \quad , \tag{11}$$

which does not contain R_s. Dividing this equation by the current yields an auxiliary function, which we call G, defined by:

$$G \equiv D/I \approx n\,v_{th}\left\{\ln(I) - [\ln(I_0) + 2]\right\} \quad . \tag{12}$$

Since this function G is calculated from function D, it requires a numerical integration of the experimental data. When G is plotted against $\ln(I)$, according to (12) the resulting curve is a straight line, whose intercept and slope allow the immediate extraction of the values of I_0, and n, respectively as is shown in Fig. 7. The extracted values of n=1.03 and I_0=0.55 nA are very close to those previously obtained by lateral optimization.
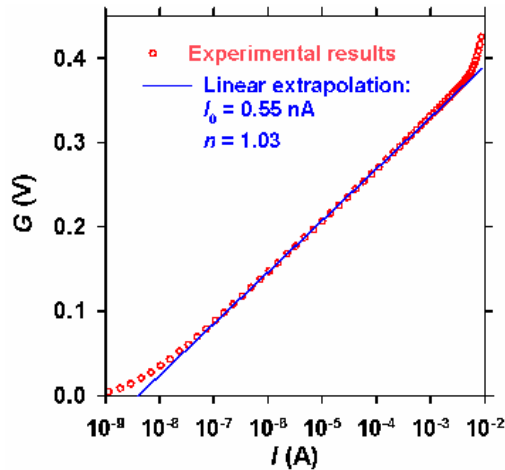

Fig. 7 Function G as a function of the logarithm of the current calculated from the measured *I*-*V* characteristics of a silicon diode (symbols) and a linear fit of its quasi linear portion (solid line)

2.2.4. *Norde's method*

This method [42] contains clever mathematical ideas and it was developed for Schottky diodes with n=1. The following notation is adapted to conventional p-n junctions. Norde defined the following function which we denominate by his name:

$$Norde = \frac{V}{2} - v_{th} \ln\left(\frac{I}{I_x}\right) \quad . \tag{13}$$

where I_x represents an arbitrary value of the current.

Norde's function presents a minimum value (V_{min}, I_{min}) which is independent on the selected value of I_x. The location of this minimum value is obtained by differentiating the above equation and equating it to zero:

$$\frac{d\,Norde}{d\,V} = \frac{1}{2} - \frac{v_{th}}{I}\frac{d\,I}{d\,V} = 0 \tag{14}$$

The derivative of V with respect to I is obtained from (5), and using $n=1$ yields:

$$\frac{d\,V}{d\,I} = R_s + \frac{v_{th}}{I} \quad . \tag{15}$$

Combining and solving the two previous equations at $I=I_{min}$ yields the series resistance:

$$R_s = \frac{v_{th}}{I_{min}} \quad . \tag{16}$$

Using (4) with $n=1$, the reverse current parameter I_0 is obtained:

$$I_0 = \frac{I_{min}}{\left[\exp\left(\frac{V_{min} - I_{min}\,R_s}{v_{th}}\right) - 1\right]} \quad , \tag{17}$$

where V_{min} is the value of the voltage at the minimum of Norde's function.

There are two main disadvantages of Norde's method: 1) that the ideality factor n needs to be assumed to be equal to unity, and 2) that the parameters are extracted from only a few data points near the minimum of Norde's function. Nevertheles, this is a clever transition.type extraction method, which extracts the parameters from a region where both the diode and the resistance effects are significant.

To test Norde's method, we will use the same previous experimental data [25], whose parameters previously were $I_0 = 0.580$ nA , $n = 1.05$ and $R_s = 33.4\ \Omega$. Since $n = 1.05$ and for the present method it should be unity, we will let v_{th}= 1.05x0.259 V. The extracted values are: $R_s = 40\ \Omega$ and $I_0 = 0.76$ nA, for the three selected values of I_x, as illustrated in Figure 8.

Figure 9 presents measured and simulated I-V characteristics, using the parameters extracted by Norde's method. We observe that simulations agrees very well with experimental data for values close to $V_{min} = 0.4$ V.
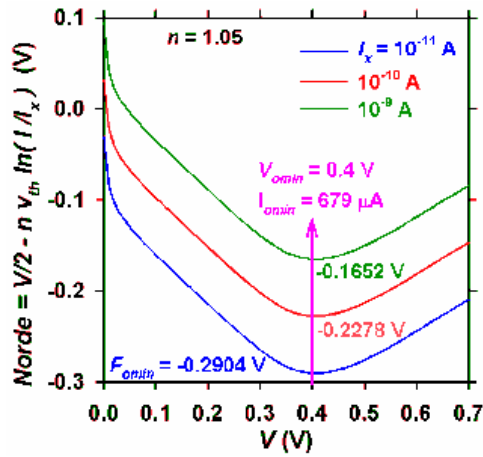
Fig. 8 Norde's function as a function of the voltage calculated from the *I-V* characteristics of the silicon diode for three values of I_x, showing the minimum that defines the value of the series resistance
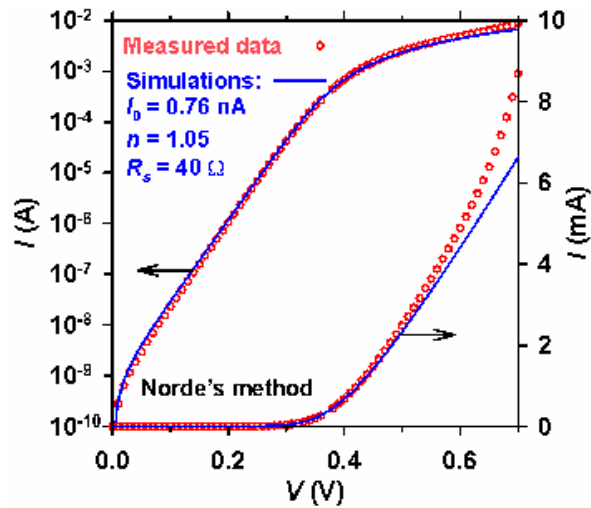

Fig. 9 Measured (symbols) and simulated (solid lines) *I-V* characteristics of the silicon diode using the parameters extracted by Norde's method

One of the limitations of Norde's method, namely that of having to fix *n*=1, has been removed by various authors [43]-[45]. For example, the following generalized Norde's function has been proposed [43], [44]:

$$Norde_\gamma = \frac{V}{\gamma} - v_{th} \ln\left(\frac{I}{I_x}\right) \quad , \tag{18}$$

where γ is a new parameter, which for the particular case of $\gamma=2$ yields the original Norde's equation. This function presents a minimum value (V_{min}, I_{min}) which is also independent on the selected value of I_x. The location of the minimum is obtained as before by differentiating (18) and equating it to zero:

$$\frac{d\,Norde_{\gamma}}{d\,V} = \frac{1}{\gamma} - \frac{v_{th}}{I}\frac{d\,I}{d\,V} = 0 \quad . \tag{19}$$

The derivative of V with respect to I is obtained from (5):

$$\frac{d\,V}{d\,I} = R_s + \frac{n\,v_{th}}{I} \quad . \tag{20}$$

Combining and solving the two previous equations at $I=I_{min}$ yields:

$$R_s = \frac{(\gamma - n)v_{th}}{I_{min}} \quad . \tag{21}$$

Using (4), the reverse current parameter I_0 is obtained:

$$I_0 = \frac{I_{min}}{\left[\exp\left(\dfrac{V_{min} - I_{min}\,R_s}{n\,v_{th}}\right) - 1\right]} \quad , \tag{22}$$

where V_{min} is the value of the voltage at the minimum of Norde's function. Because there are only two equations available ((21) and (22)), and we need to extract 3 parameters (n, I_0 and R_s), at least two Norde's plots with different values of γ are needed.

It is interesting to compare the generalized Norde's function with the previous G function. If we make γ tend to infinity and let $I_x = I_0$, the generalized Norde's function *is closely related to* the G function by:

$$Norde_{\substack{\gamma=\infty \\ I_x=I_0}} = -\frac{G}{n} \quad . \tag{23}$$

2.2.5. *Cheung's method*

Cheung et al [45] proposed the following procedure to extract the idelity factor and the series resistance. Using the identity:

$$\frac{d\,V}{d\,\ln(I)} = I\frac{d\,V}{d\,I} = \frac{I}{\dfrac{d\,I}{d\,V}} \tag{24}$$

in combination with equation (20) yields:

$$\frac{I}{\dfrac{d\,I}{d\,V}} = R_s\,I + n\,v_{th} \quad . \tag{25}$$

Therefore, when the ratio of the current to the conductance ($I/(\mathrm{d}I/\mathrm{d}V)$) is plotted against the current it should produce a straight line, as shown in Figure 10, whose slope yields the series resistance and its intercept is nv_{th}, implying in the example shown that $R_s = 33.3$ Ω and $n = 1.17$.
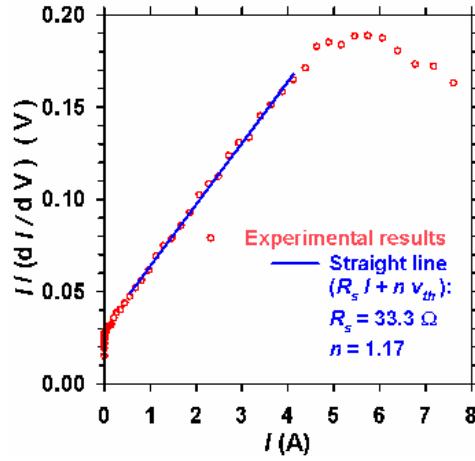

Fig. 10 Ratio of the current to the conductance (I/(dI/dV)) as a function of the current showing a straight line behaviour

Cheung et al proposed the following variation of Norde's function [45]:

$$Cheung = V - n\,v_{th}\,\ln\!\left(\frac{I}{I_x}\right).$$
(26)

where I_x is an arbitrary value of the current. Rewriting (5) with the assumption $I \gg I_0$ yields:

$$V = R_s\,I + n\,v_{th}\,\ln\!\left(\frac{I}{I_0}\right).$$
(27)

Combining the two previous equations yields:

$$Cheung = R_s\,I + nv_{th}\,\ln\!\left(\frac{I_x}{I_0}\right).$$
(28)

Therefore, when Cheung's function is plotted against the current it should produce a straight line, as is shown in Figure 11, whose slope yields the series resistance and its intercept the reverse current, implying in the present example shown that $R_s = 33.4$ Ω and $I_0 = 2.6$ nA.
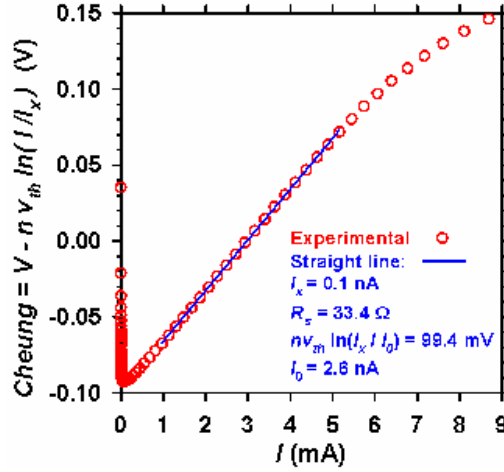
Fig. 11 Cheung's function as a function of the current showing a straight line behaviour

2.3. Single-exponential diode model with series and parallel resistances

Figure 12 presents the lumped parameter equivalent circuit model of a diode with a series parasitic resistance and two parallel parasitic conductances, one at the junction (G_{p1}) and the other at the periphery (G_{p2}). The mathematical description of the terminal current of this equivalent circuit is given by the implicit equation:

$$I = I_0 \left\{ \exp\left[\frac{V\,(1 + R_s G_{p2}) - I R_s}{n\,v_{th}} \right] - 1 \right\} + (V - I R_s) G_{p1} + V G_{p1}(1 + R_s G_{p1}) \quad . \qquad (29)$$

The above equation has the following solution for the terminal current as a function of the terminal voltage [46], [47]:

$$I = \frac{n v_{th}}{R_s} W_0 \left\{ \frac{I_0 R_s}{n v_{th}(1 + R_s G_{p1})} \exp\left[\frac{(V + I_0 R_s)}{n v_{th}(1 + R_s\,G_{p1})} \right] \right\} + \left(\frac{V\,G_{p1} - I_0}{1 + R_s\,G_{p1}} \right) + V\,G_{p2} \quad , \qquad (30)$$

and for the terminal voltage as a function of the terminal current the solution is:

$$V = -n v_{th}\,d_2\,W_0 \left\{ \frac{I_0\,R_{12}}{n v_{th}\,d_2} \exp\left[\frac{\left(I + \dfrac{I_0}{d_2} \right) R_{12}}{n v_{th}} \right] \right\} + I\,d_2\,(R_s + R_{12}) + I_0\,R_{12} \quad , \qquad (31)$$

where W_0 represents the principal branch of the *Lambert W* function, and

$$d_1 \equiv 1/(1+R_s \ G_{p1}) \quad , \tag{32}$$

$$d_2 \equiv 1/(1+R_s \ G_{p2}) \quad , \tag{33}$$

and

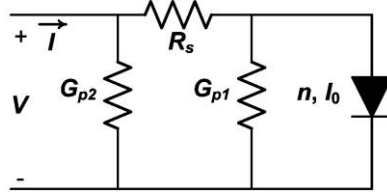$$R_{12} \equiv 1/(G_{p1} +G_{p2} + G_{p1}G_{p2} \ R_s) \quad . \tag{34}$$

Fig. 12 Lumped parameter equivalent circuit model with a parasitic series resistance and two parallel parasitic conductances, representing two possible shunt current losses, one at the junction (G_{p1}) and another at the device's periphery (G_{p2})

2.3.1. Bidimensional fit of function D

This integration-based procedure that was developed in 2005 [47] can be summarized as follows: First for convenience function D in (10) is rewriten as:

$$D(V,I) = 2\int_0^I V \, dI - IV \quad . \tag{35}$$

Secondly the terminal voltage given by (31) and its integral with respect to I are substituted into (35), which results in a long expression that contains *Lambert W* functions and the variables V and I. Thirdly, substituting all the terms that contain *Lambert W* functions using equation (31), and after some algebraic manipulations, we can arrive at a form of function $D(I,V)$ that is conveniently expressed as the following purely algebraic bivariate equation:

$$D(I,V) = D_{V1}V + D_{I1}I + D_{V1I1}VI + D_{V2}V^2 + D_{I2}I^2 \quad , \tag{36}$$

where the five coefficients are given by:

$$D_{I1} = -2R_s I_0 - 2n v_{th} \ (1+G_{p1}R_s) \quad , \tag{37}$$

$$D_{V1} = 2R_s n v_{th} G_{p1}G_{p2} + 2I_0(R_s G_{p2} +1) + 2n v_{th}(G_{p1} + G_{p2}) \quad , \tag{38}$$

$$D_{I2} = -R_s (1+G_{p1}R_s) \quad , \tag{39}$$

$$D_{V2} = -G_{p2} - G_{p1} - 2R_s G_{p1}G_{p2} - R_s G_{p2}^2 - R_s^2 G_{p1}G_{p2}^2 \quad , \tag{40}$$

and the fifth coefficient is dependent upon the others:

$$D_{I1V1}^2 = 1+4 \ D_{I2} \ D_{V2} \quad . \tag{41}$$

As can be seen, there are actually four independent coefficients, (37)-(40), and therefore only four unknowns may be extracted uniquely. The general solution of n, I_0, G_{p1}, and G_{p2}, in terms of R_s, D_{I1}, D_{V1}, D_{I2} and D_{V2} is:

$$G_{p1} = -\frac{D_{I2} + R_s}{R_s^2} \quad , \tag{42}$$

$$n = -\frac{R_s D_{V1} + R_s G_{p2} D_{I1} + D_{I1}}{2\, v_{th}} \quad , \tag{43}$$

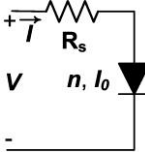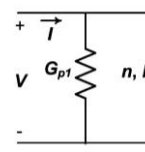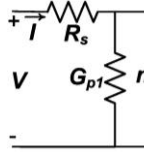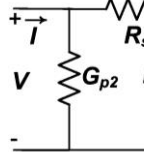$$G_{p2} = -\frac{-1 - 2 R_s G_{p1} + \sqrt{1 - 4 R_s D_{V2} - 4 R_s^2 G_{p1} D_{V2}}}{2 R_s (1 + R_s G_{p1})} \quad , \tag{44}$$

and

$$I_0 = \frac{1}{2}(D_{V1} + G_{p1} D_{I1} + G_{p2} D_{I1} + G_{p1} R_s D_{V1} + G_{p1} R_s G_{p2} D_{I1}) \quad . \tag{45}$$

It is important to notice that a set of values of D_{I1}, D_{V1}, D_{I2} and D_{V2} defines a unique *I-V* characteristic which can be generated with various combinations of R_s, n, I_0, G_{p1}, and G_{p2}. Particular cases, which do not simultaneously include both conduntances G_{p1} and G_{p2}, present specific solutions as presented in Table 1. The parameter extraction procedure consists of fitting algebraic equation (36) to the $D(I,V)$ function as numerically calculated from the experimental data with (35). This bidimensional (bivariate) fitting process produces the values of the equation coefficients D_{V1}, D_{I1}, D_{V2}, D_{I2}. These resulting values are then used to calculate the diode model parameters (G_{p1} or G_{p2}, R_s, n, and I_0), as presented in Table 1 for the particular cases.

To illustrate this extraction method, it was applied to simulated *I-V* characteristics for the case of series resistance and only peripheral shunt loss, using parameters values of I_0 = 1 pA, n = 1.5, G_{p1} = 0 and various combinations of R_s and G_{p2} as is shown in Figure 13. Symbols used in this figure are not data points but are used to identify the several cases. The ideal case of R_s = 0 and G_{p2} = 0, identified by large hollow squares, is a straight line. The case when R_s = 1kΩ is significant and G_{p2} = 0, identified by small solid squares, produces a straight line for low voltage that bends down for high voltage (i.e. the effects R_s become important at high voltage). The case when only G_{p2} is significant (G_{p2} = 1μS and R_s = 0), is identified by small solid circles. It is a straight line at high voltage and bends up at low voltage (i.e. the effects G_{p2} are important at low voltage). When R_s and G_{p2} are both simultaneously significant (R_s = 1kΩ and G_{p2} = 1μS) is identified by large hollow circles. It is important to notice that the plot in this extreme case does not exhibit any region from which the intrinsic parameters could be obtained, because the overlapping effects of R_s and G_{p2} totally conceal the intrinsic characteristics everywhere. This contrasts with the fact that the intrinsic parameters of this extreme case could not be directly extracted by any traditional method from any portion of its *I-V* characteristics.

Table 1 Particular cases of a single-exponential diode model

D_{V1}	$2I_0$	$2I_0+2nv_{th}G_{p1}$	$2I_0+2nv_{th}G_{p1}$	$2I_0(R_sG_{p2}+1)+2nv_{th}G_{p2}$
D_{I1}	$-2R_sI_0-2nv_{th}$	$-2nv_{th}$	$-2R_sI_0-2nv_{th}(1+G_{p1}R_s)$	$-2R_sI_0-2nv_{th}$
D_{V2}	0	$-G_{p1}$	$-G_{p1}$	$-G_{p2}(1+R_sG_{p2})$
D_{I2}	$-R_s$	0	$-R_s(1+G_{p1}R_s)$	$-R_s$
G_{p1}	0	$-D_{V2}$	$-D_{V2}$	0
G_{p2}	0	0	0	$\dfrac{-1+\sqrt{1-4R_sD_{V2}}}{2R_s}$
R_s	$-D_{I2}$	0	$\dfrac{-1+\sqrt{1-4G_{P1}D_{I2}}}{2G_{P1}}$	$-D_{I2}$
n	$-\dfrac{D_{I1}+2R_sI_0}{2v_{th}}$	$-\dfrac{D_{I1}}{2v_{th}}$	$-\dfrac{D_{I1}+R_SD_{V1}}{2v_{th}}$	$-\dfrac{2R_sI_0+D_{I1}}{2v_{th}}$
I_0	$\dfrac{D_{V1}}{2}$	$\dfrac{D_{V1}-2nv_{th}G_{p1}}{2}$	$\dfrac{D_{V1}-2nv_{th}G_{P1}}{2}$	$\dfrac{D_{I1}G_{P2}+D_{V1}}{2}$

The previously described combinations, as well as several other additional cases, were simulated and the quadratic equation of D as a function of current and voltage, defined in (36), was then used to extract the simulated parameters. In all cases the extraction procedure succeeded in producing the exact original parameters, within computational accuracy. This means that the errors between the original and the extracted parameters depend only on the computational precision and accuracy of the fitting algorithms used. It must be pointed out that in order to obtain reasonably accurate results, it is advisable that measurements use a small as possible voltage step (typically at most 10 mV). Additionally, it is of paramount importance to use a suitable algorithm for numerical integration, that is, one that will not introduce significant error, such as a closed Newton-Cotes formula with 7 points, as illustrated in the Appendix of [41].
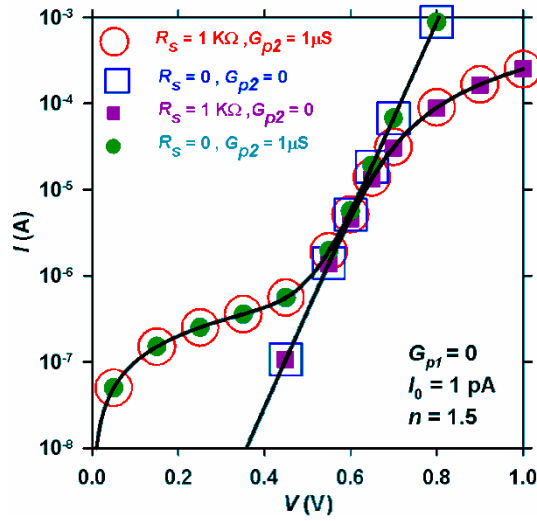

Fig. 13 Illustrative synthetic *I-V* characteristics for various cases with several series resistance values and several peripheral shunt loss values. Symbols are used to identify the several cases and do not represent data points

2.3.2. *Iterative G function method*

For the particular case of $G_{p1}=0$ an iterative procedure was proposed in 2000 [48], which is based on the *G* function described in Section 2.2.3. By estimating the value of G_{p2} (G_{p2e}) we can calculate the current in the diode branch:

$$I_D = I - G_{p2e} V \quad . \tag{46}$$

Then, function *G* is calculated from the measured *I-V* data and is plotted as a function of $\ln(I_D)$ for different estimated values of G_{p2e}. Selecting the plot that best fits a straight line will determine the correct value of $G_{p2e}=G_{p2}$.

To illustrate the approach, we use simulated data with parameters values: $I_0=1$ pA, $n=1.5$, $R_s=1$ kΩ and $G_{p2}=1$ μS. Figure 14 presents several plots of the calculated function

G, using the I_D defined in Eq. (46), for several estimated values of G_{p2e}. The best straight line of the function G with respect to $\ln(I_D)$ will define the correct value of G_{p2e}.
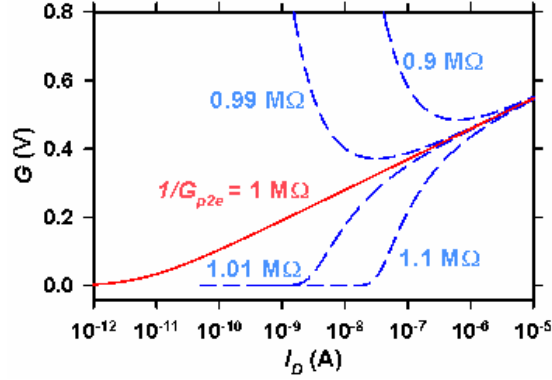

Fig. 14 Function G vs the logarithm of the I_D estimated using (46). The plots tend to a straight line (solid line) when the estimated value of G_{p2e} approaches the actual value of $G_{p2}=1\,\mu S$

3. MULTIPLE-EXPONENTIAL DIODE MODEL

When modeling real junctions a single-exponential equation is usually not enough to adequately represent the several conduction phenomena that frequently make relevant contributions to the total current of a particular junction. In such cases junctions need to be represented by lumped multi-diode equivalent circuits.

3.1. Double-exponential diode model with series resistance

The first single-exponential model for a p-n junction with a unity ideality factor and a series resistance was proposed by Shockley in 1949 [15]. In 1957, Sah et al [18] presented the first double-exponential model for a p-n junction with series parasitic resistance and diode quality factors of $n_2=2n_1$ and $n_1=1$. The lumped parameter equivalent circuit is illustrated in Fig. 15. The mathematical description of this circuit is given by the following implicit equation:

$$I = I_{01}\left[\exp\left(\frac{V-I\,R_s}{v_{th}}\right)-1\right]+I_{02}\left[\exp\left(\frac{V-I\,R_s}{2\,v_{th}}\right)-1\right] \qquad (47)$$

The above implicit equation does not have an explicit solution for the terminal current, but it does have a solution for the terminal voltage as an explicit function of the terminal current [49]:

$$V = R_s\,I + 2v_{th}\ln\left[\sqrt{\left(\frac{I_{02}}{2\,I_{01}}+1\right)^2+\frac{I}{I_{01}}}-\frac{I_{02}}{2\,I_{01}}\right] \qquad . \qquad (48)$$

A global lateral fitting procedure based on (48) has been proposed to directly extract the diode's model parameters [49]. Figure 16 presents the *I-V* characteristics of an experimental silicon PIN lateral diode fabricated at the Université Catolique de Louvain [49] measused at two temperatures. The model playback *I-V* characteristics calculated using the parameter values extracted using this global lateral fitting procedure are also shown in Fig. 16.
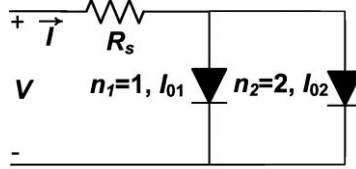

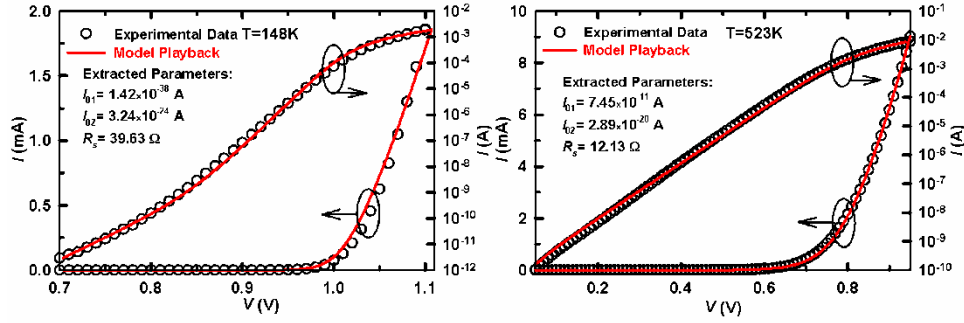**Fig. 15** A double-exponential model with series resistance

Fig. 16 Measured and simulated *I-V* characteristics of an experimental silicon lateral PIN diode at two temperatures. The playback is calculated using the double-exponential model, with diode quality factors of $n_2=2$ and $n_1=1$, and the rest of the parameter values extracted by a direct global lateral fitting of (48) to the data

It is important to point out that this lateral fitting procedure may be used in general when the value of one diode quality factor can be assumed to be roughly twice the value of the other ($n_2 \approx 2n_1$) even if $n_1 \neq 1$. It is also worth mentioning here that a double-exponential model parameter extraction method, based on area error minimization between measured and modeled *I-V* characteristics, was recently proposed by Yadir et al [50]. The essence of that method is closely related to integration-based extraction methods [23], [24].

3.2. Functions *A* and *B*

Another possible situation worth considering is represented by a double-exponential model where the values of the ideality factors are arbitrary, and all series resistances and shunt conductances are negligible, as illustrated by the equivalent circuit shown in Fig. 17. The mathematical description of the terminal current of such a circuit is given by the following explicit function of the terminal voltage:

$$I = I_{01}\left[\exp\left(\frac{V}{n_1 v_{th}}\right) - 1\right] + I_{02}\left[\exp\left(\frac{V}{n_2 v_{th}}\right) - 1\right]. \tag{49}$$

Additionally assume that diode 2 (n_2, I_{02}) is dominant at low voltage, the curren in that region may be approximated by:

$$I \approx I_{02}\left[\exp\left(\frac{V}{n_2 v_{th}}\right) - 1\right]. \tag{50}$$
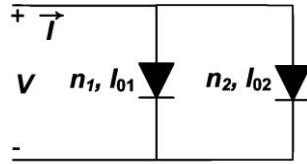

Fig. 17 Ideal double-exponential model with arbitrary ideality factors and without parasitic resistances

Substituting (50) into the following operators A and B, yields [51]:

$$A \equiv \frac{CC}{I} = \frac{\int_0^V I\,dV}{I} = n_2 v_{th} - I_{02}\left(\frac{V}{I}\right) \tag{51}$$

and

$$B \equiv \frac{CC}{V} = \frac{\int_0^V I\,dV}{V} = n_2 v_{th}\left(\frac{I}{V}\right) - I_{02}. \tag{52}$$

Therefore, the application of either one of these two operators (51) or (52) to measured I-V characteristics produces linear equations on the ratio V/I or on its reciprocal I/V, from whose slopes and intercepts the values of the ideality factor n_2 and the reverse saturation current I_{02} may be directly extracted.

Figure 18 presents measurements of the base current as a function of forward base-emitter voltage of a power BJT measured at T =298 K with V_{BC}=0. Figure 19 shows plots of operators A and B applied to this measurements. The slope of A gives an extracted value of I_{02}=215 pA, and its ordinates axis intercept gives an extracted value of n_2=2. The slope of function B gives an extracted value of n_2=1.98, and its ordinates axis intercept gives an extracted value of I_{02} =210 pA. It is worth mentioning that a vertical optimization method could also be used for this case, as is illustrated in Fig. 20.
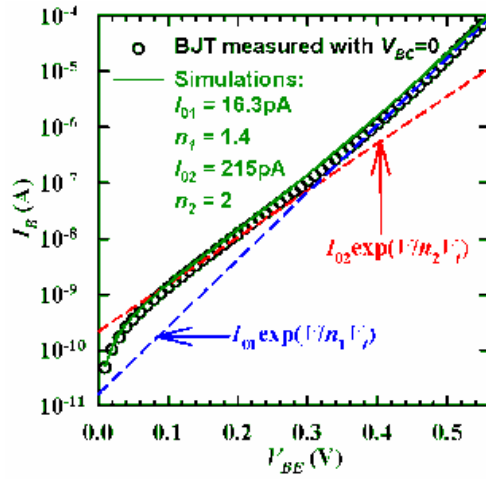
Fig. 18 Measured characteristics (symbols) of the base current as a function of forward base-emitter voltage of a power BJT measured at T =298 K, with V_{BC}=0 and 10 mV voltage steps. Also shown is the model playback simulated with (49) (solid line). The low and high voltage asymptotes (dashed lines) are also shown
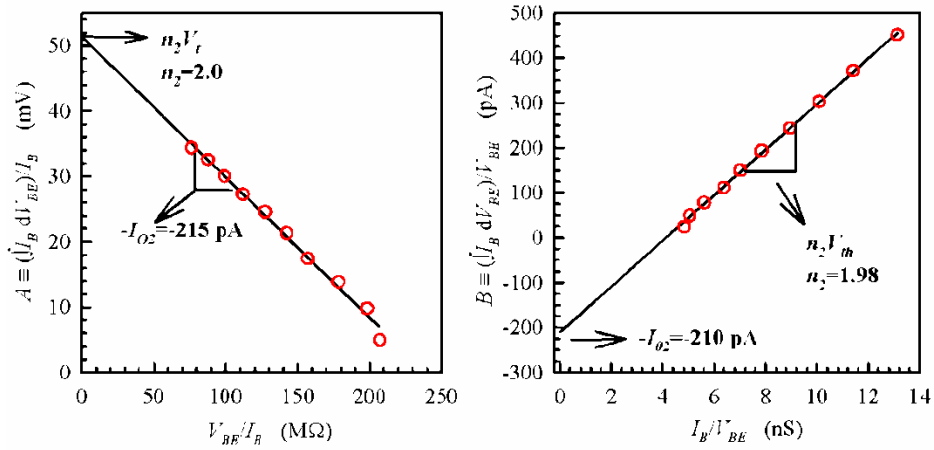

Fig. 19 Plots of operators A (51) and B (52) applied to the measured power BJT characteristics shown in Fig. 18
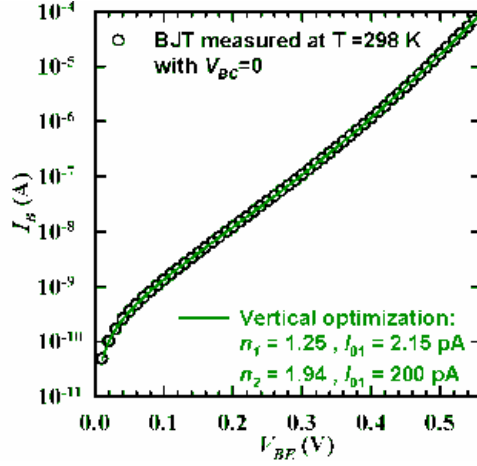
Fig. 20 Measured characteristics (symbols) of the power BJT shown in Fig. 18, and the model playback simulated with (49) (solid line) using the parameter values extracted by vertical optimization

3.3. Regional approach for a double diode with series and parallel resistance

This method is based on the idea that some components of the diode model dominate at a given voltage region [39]. Let us assume a double-exponential model with arbitrary values of ideality factors and with parallel and series resistance as illustrated in Figure 21. The mathematical description of this circuit is given by the following explicit equation:

$$I = I_{01}\left[\exp\left(\frac{V - I R_S}{n_1 V_{th}}\right) - 1\right] + I_{02}\left[\exp\left(\frac{V - I R_S}{n_2 V_{th}}\right) - 1\right] + G_p(V - I R_S) \quad . \tag{53}$$
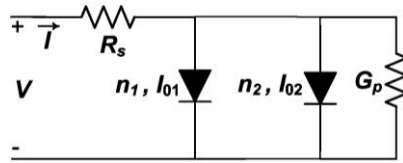
Fig. 21 Double-exponential model with arbitrary ideality factors and parasitic series and parallel resistances

Figure 22 presents a particular simulation using (53) with specific parameter values in which we observe that for low voltage, diode 2 and G_p are dominant. Thus, equation (53) may be simplified for low voltages to the following explicit equation:

$$I \approx I_{02}\left[\exp\left(\frac{V}{n_2 V_{th}}\right) - 1\right] + G_p V \quad , \tag{54}$$
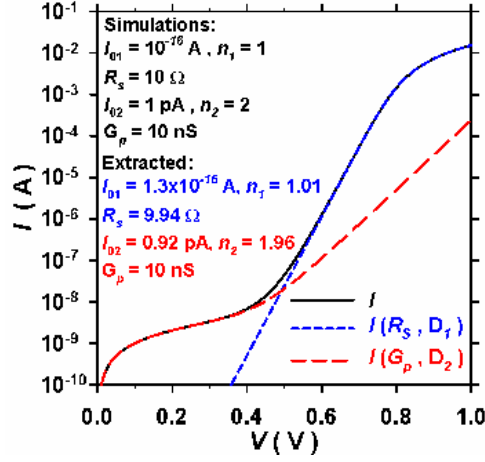
Fig. 22 Synthetic *I-V* characteristics simulated by (53) with the parameter values
indicated inside the figure, together with the components dominant at low and
high voltage, as calculated with the parameter values locally extracted using (54)
and (56) (also indicated inside the figure)

Similarly, for high voltage, diode 1 and R_s are dominant, thus equation (53) may be
simplified for high voltages to to the following implicit equation:

$$I \approx I_{01} \left[\exp\left(\frac{V - I R_S}{n_1 V_{th}} \right) - 1 \right] \quad , \tag{55}$$

Although (55) is implicit, it has the following explicit solution for the terminal voltage:

$$V = R_s I + n_1 v_{th} \ln\left(1 + \frac{I}{I_{01}} \right) \quad . \tag{56}$$

Therefore, the parameters can be extracted locally from two regions: 1) G_p, n_2 and I_{02} by
vertical optimization of the low voltage region fitting equation (54) to the measured
current; and 2) R_s, n_1 and I_{01} by by lateral optimization of the high voltage region fitting
equation (56) to the measured voltage. Figure 22 also includes the original and the
parameter values extracted by this method.

3.4. Alternative multi-exponential model with parasitic resistances

Figure 23 illustrates a multi-diode equivalent circuit. Accordingly, the total current
has been traditionally described by the following conventional implicit equation:

$$I = \sum_{k=1}^{N} I_{0k} \left[\exp\left(\frac{V - R_s I}{n_k v_{th}} \right) - 1 \right] + G_p (V - R_s I) \quad . \tag{57}$$
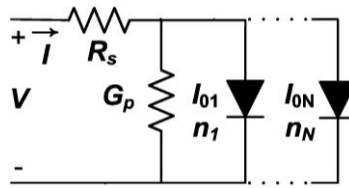
Fig. 23 A conventional equivalent circuit of a real junction with multiple diodes

In order to circumvent the explicit insolvability of the previous equation, we proposed [52] the use of the equivalent circuit presented in Figure 24. By solving each branch separately and adding the solutions, this model's *I-V* characteristics may be expressed by the following explicit equation for the terminal current:

$$I = \sum_{k=1}^{N} \left\{ \frac{n_{ka} v_{th}}{R_{ska}} W_0 \left[\frac{R_{ska} I_{0ka}}{n_{ka} v_{th}} \exp\left(\frac{V + R_{ska} I_{0ka}}{n_{ka} v_{th}} \right) \right] - I_{0ka} \right\} + G_{pa} V \ . \quad (58)$$

where as before W_0 represents the principal branch of the *Lambert W* function [31], $G_{pa} = 1/R_{pa}$ is the alternative outer shunt conductance and the rest of the parameters are defined as before. Notice that the single global series resistance, R_s, present in the conventional model, has been substituted in this alternative model by individual series resistances, R_{ska}, placed in each of the kth parallel current paths associated with the kth conduction mechanism.
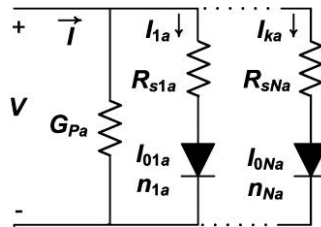
Fig. 24 Alternative equivalent circuit with multiple diodes, resistances in series with each diode, and an outer shunt resistance

Figure 25 presents the *I-V* characteristics of a lateral PIN diode at four temperatures from 300 to 390 K. Model parameters were extracted, for both conventional and alternative double-exponential models, by globally fitting the logarithm of each model to the experimental data. The left figure also includes the corresponding alternative model playbacks while the right figure includes the corresponding conventional model playbacks. Additional calculations of the playback errors relative to the original measured data indicate that the alternative model produces a more accurate representation of this device's forward conduction behavior at the four temperatures considered here.

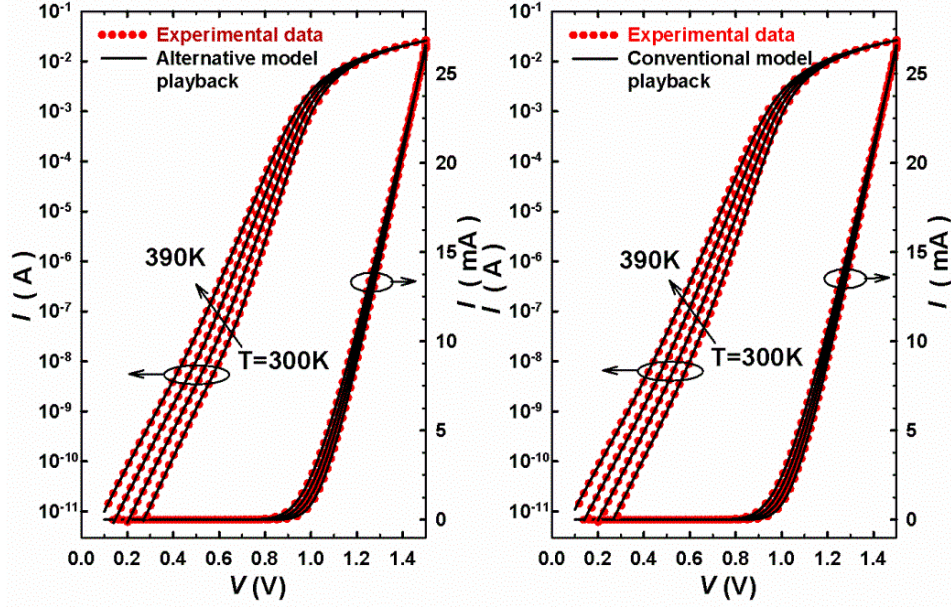**Fig. 25** Measured (red symbols), alternative and conventional model playbacks (black solid lines) forward *I–V* characteristics of an experimental lateral PIN diode at four temperatures

3.5. Lateral optimization using an approximate analytical expression for the voltage in multi-exponential diode models

Whenever the conductance G_p can be neglected in the model presented in Fig. 23, the total current is described by the following conventional implicit equation:

$$I = \sum_{k=1}^{N} I_{0k} \left[\exp\left(\frac{V - R_s I}{n_k v_{th}} \right) - 1 \right]. \tag{59}$$

We recently proposed [53] an approximate solution of the above transcendental equation for the terminal voltage as an explicit function of the terminal current valid for arbitrary *N*, I_{0k}, and n_k. This approximate solution is [53]:

$$V \approx R_s I - m v_{th} \ln \left[\sum_{k=1}^{N} \left(\frac{I}{I_{0k}} + 1 \right)^{-\frac{n_k}{m}} \right]. \tag{60}$$

where *m* represents an empiric dimensionless joining factor. It is important to note in (60) that at a any particular bias point (*I, V*) at which only one of the conduction mechanisms represented by one of the diodes in the model is dominant, the summation in (60) reduces to only one term. For the particular case of a model with just two parallel diodes (*N*=2)

with arbitrary values of n_1 and n_2, the explicit approximate terminal voltage solution simplifies to:

$$V \approx R_s\, I - m\, v_{th} \ln\left[\left(\frac{I}{I_{01}}+1\right)^{-\frac{n_1}{m}} + \left(\frac{I}{I_{02}}+1\right)^{-\frac{n_2}{m}}\right]. \tag{61}$$

To illustrate the applicability of this approximate model, we applied it to experimental *I–V* characteristics of lateral thin-film SOI PIN diodes. Figure 26 presents the measured *I–V* characteristics of a device where parameter extraction was performed using lateral optimization by minimizing voltage errors at a given current. The extracted parameters and the joining factor are indicated in Fig. 26, together with the lateral voltage error with respect to measured data.
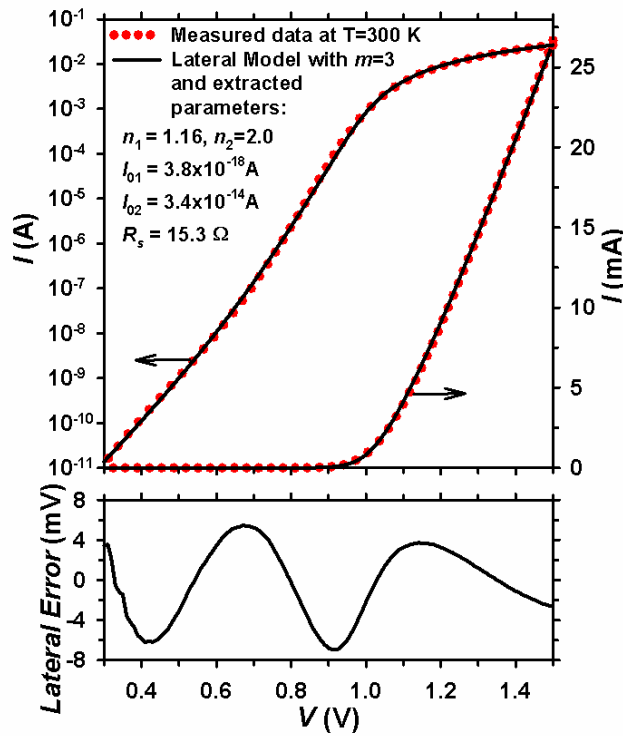

Fig. 26 (Upper pane) Measured (red dotted lines) and model playback (black solid lines) of a lateral thin-film SOI PIN diode at 150 K in linear and logarithmic scales; and (lower pane) absolute lateral error of model playback with respect to the measured data

4. SINGLE-EXPONENTIAL SOLAR CELL MODEL

4.1. Single-exponential model without any resistance

Consider an idealized solar cell without any parasitic resistance, whose *I-V* characteristics under illumination may be described by superposition of two currents: a voltage independent photo-generated current source and the current of a single exponential-type junction, as shown in Fig. 27.
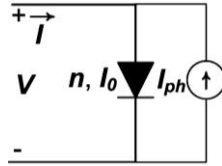
Fig. 27 Idealized solar cell equivalent circuit without parasitic resistances

The terminal current of this lumped parameter equivalent circuit model is mathematically described by the following explicit equation of the terminal voltage:

$$I = I_0 \left[\exp\left(\frac{V}{n v_{th}} \right) - 1 \right] - I_{ph} \tag{62}$$

where the magnitude of the photo-generated current I_{ph} depends only on the illumination intensity. Alternatively the terminal voltage may be expressed as an explicit function of the terminal current:

$$V = n v_{th} \ln\left(1 + \frac{I + I_{ph}}{I_0} \right) \tag{63}$$

Figure 28 shows simulated *I-V* characteristics of an idealized solar cell, in linear and logarithmic scales, under illumination.

Fig. 28 Simulated dark and illuminated *I-V* characteristic of an idealized solar cell in linear and logarithmic scales

The short circuit current (I_{SC}) and open circuit voltage (V_{OC}) can be found by evaluating (62) at $V=0$ and (63) at $I=0$, respectively, as:
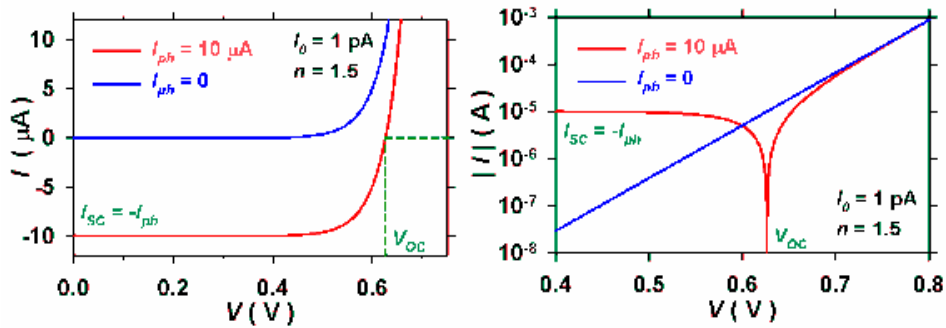
$$I_{SC} \equiv I\big|_{V=0} = -I_{ph} \quad , \tag{64}$$

and

$$V_{OC} \equiv V\big|_{I=0} = n v_{th} \ln\left(1+\frac{I_{ph}}{I_0}\right) \quad . \tag{65}$$

The output power is given by the $V{\cdot}I$ product. Using (6.1) yields:

$$P = V\,I = V\left\{ I_0\left[\exp\left(\frac{V}{n v_{th}}\right)-1\right]-I_{ph}\right\} \quad . \tag{66}$$

Maximum output power will be delivered when (66) becomes maximun. Differentiating (66) with respect to voltage and equating to zero yields the value of the voltage (V_{mpp}) at the maximum power point (MPP):

$$V_{mpp} = n v_{th}\left[W_0\left(\frac{2.718\left(I_0+I_{ph}\right)}{I_0}\right)-1\right] \approx n v_{th}\left[W\left(\frac{2.718 I_{ph}}{I_0}\right)-1\right] \quad , \tag{67}$$

where W_0 stands for the principal branch of the *Lambert W* function [31]. The corresponding current (I_{mpp}) at the MPP is found by evaluating (62) at V_{mpp} using (67).

4.2. Single-exponential model with series resistance

Figure 29 presents the lumped parameter equivalent circuit model of a solar cell with parasitic series resistance.
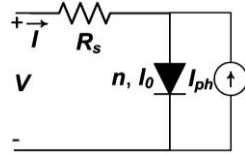
Fig. 29 Solar cell equivalent circuit with a parasitic series resistance

As a consequence of the presence of the parasitic series resistance R_s, the terminal current of this equivalent circuit is mathematically described by an implicit equation:

$$I = I_0\left[\exp\left(\frac{V-R_s I}{n v_{th}}\right)-1\right]-I_{ph} \quad . \tag{68}$$

The terminal voltage can be mathematically solved from (68) resulting in an explicit function of the terminal current:

$$V = R_s\, I + n\, v_{th}\, \ln\left(1 + \frac{I + I_{ph}}{I_0}\right) .$$ (69)

The implicit terminal current equation given by (68) can be solved explicitly in terms of the terminal voltage if we introduce the use of the special *Lambert W* function [54]:

$$I = \frac{n v_{th}}{R_s}\, W_0\left\{\frac{I_0 R_s}{n v_{th}}\exp\left[\frac{V + R_s(I_0 + I_{ph})}{n v_{th}}\right]\right\} - (I_0 + I_{ph}) .$$ (70)

Another consequence of the presence of the parasitic series resistance R_s is that it prevents finding an exact analytical solution for the maximum power point, since equating the derivative of the *VI* product to zero does not allow to analytically solve for either V_{mpp} or I_{mpp}.

Figure 30 illustrates the effect of series resistance R_s on linear and semilogarithmic scale *I-V* characteristics simulated under illumination with three values of R_s.
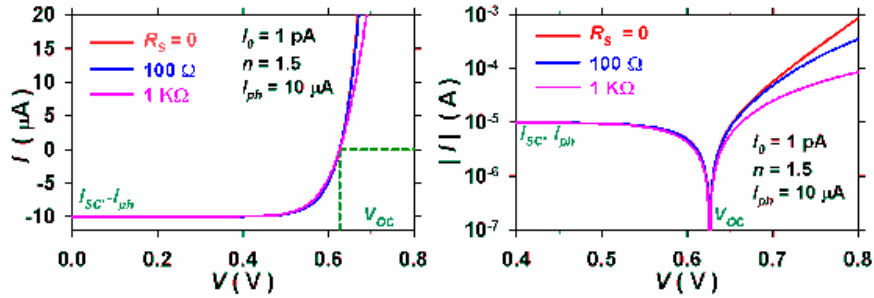

Fig. 30 Simulated *I-V* characteristic of a solar cell at different values of parasitic series resistance, in linear and logarithmic scale

The open circuit voltage V_{OC} does not depend on R_S, since its effect, given by $I \cdot R_S$, becomes zero when the current goes to zero (open circuit). Thus, the value of V_{OC} is given by the same equation (65). On the other hand, the short circuit current I_{SC} can be found by evaluating (70) at $V=0$, as:

$$I_{SC} \equiv I\big|_{V=0} = \frac{n v_{th}}{R_s}\, W\left\{\frac{I_0 R_s}{n v_{th}}\exp\left[\frac{R_s(I_0 + I_{ph})}{n v_{th}}\right]\right\} - (I_0 + I_{ph}) .$$ (71)

The four parameters (n, I_0, R_S and I_{ph}) that fully describe the solar cell in terms of this lumped parameter equivalent circuit model can be extracted by fitting the cell's measured data to any of the model's defining equations. Equations (68), (69) or (70) can be applied directly for fitting. Vertical or lateral optimization could be used for fitting by minimizing either the voltage quadratic error or the current quadratic error, respectively. In the present case the use of equation (69) in combination with lateral optimization affords the best computational convenience, since this equation is not implicit, as (68) is, and does not contain special functions, as (70) does.

4.2.1. *First integration method to extract the series resistance of solar cells*

To the best of our knowledge, Araujo and Sánchez were the first to propose, back in 1982, the use of integration for parameter extraction in solar cells [36]. They used the integral of (69), assuming that $I \gg I_0$ and $I_{ph} \gg I_0$, to obtain the relation:

$$\int_0^I V \, dI \approx \frac{R_s}{2} I^2 - n v_{th} I + n v_{th} \left(I + I_{ph} \right) \ln\left(\frac{I + I_{ph}}{I_0} \right) - n v_{th} I_{ph} \ln\left(\frac{I_{ph}}{I_0} \right). \quad (72)$$

Evaluating (72) at an upper limit of integration $I=I_{SC}$, the series resistance R_s can be evaluated as:

$$R_s \approx 2 \frac{\int_0^{I_{sc}} V \, dI}{I_{SC}^2} + 2 \frac{n v_{th}}{I_{SC}} - 2 \frac{V_{OC}}{I_{SC}} . \quad (73)$$

4.3. Single-exponential model with parallel resistance

Figure 31 presents the lumped parameter equivalent circuit model of a solar cell with parallel series resistance.

Fig. 31 Solar cell lumped parameter equivalent circuit model with parasitic parallel conductance

The mathematical description of the terminal current of this equivalent circuit is given in terms of the terminal voltage by the explicit equation:

$$I = I_0 \left[\exp\left(\frac{V}{n v_{th}} \right) - 1 \right] - I_{ph} + G_p V . \quad (74)$$

The terminal voltage can be solved from the above equation as an explicit function of the terminal current if we use the special *Lambert W* function:

$$V = - n v_{th} W_0 \left[\frac{I_0}{n v_{th} G_p} \exp\left(\frac{I + I_0 + I_{ph}}{n v_{th} G_p} \right) \right] + \frac{I + I_0 + I_{ph}}{G_p} . \quad (75)$$

As a consequence of the presence of the parallel conductance G_p an exact analytical solution for the maximum power point is not possible, since equating the derivative of the $V \cdot I$ product to zero does not allow to analytically solve for either V_{mpp} or I_{mpp}. Figure 32 illustrates the effect of parallel conductance G_p on linear and semilogarithmic scale I-V characteristics simulated under illumination with three values of G_p.
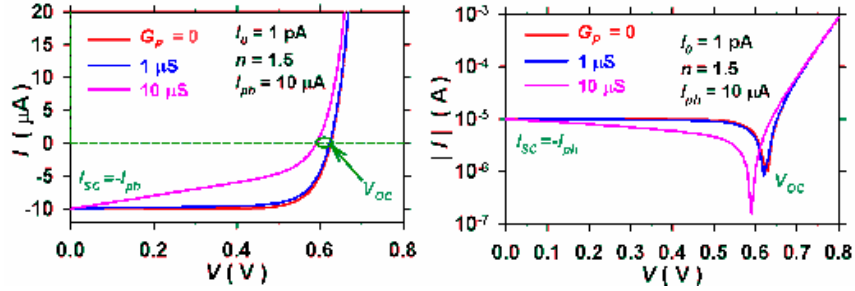
Fig. 32 Simulated *I-V* characteristic of a hypothetical solar cell for three values of parallel conductance in linear and logarithmic scales

For this particular case we find the short circuit current by evaluating (74) at *V*=0, yielding $I_{SC} = -I_{ph}$, which is independent of the value of G_p. The open circuit voltage V_{OC} is obtained by evaluating (75) at *I*=0, yielding:

$$V_{OC} = - n v_{th} W\left[\frac{I_0}{n v_{th} G_p} \exp\left(\frac{I_0 + I_{ph}}{n v_{th} G_p}\right)\right] + \frac{I_0 + I_{ph}}{G_p} \quad . \tag{76}$$

The four parameters (n, I_0, G_p and I_{ph}) that fully describe the solar cell in terms of this lumped parameter equivalent circuit model can be extracted by fitting the cell's measured data to any of the model's defining equations. Equations (74) or (75) can be applied directly for fitting. Vertical or lateral optimization could be used for fitting by minimizing either the voltage quadratic error or the current quadratic error, respectively. In the present case the use of equation (74) in combination with vertical optimization affords the best computational convenience, since this equation is explicit and does not contain special functions, as (75) does.

4.4. Single-exponential model with series and parallel resistances

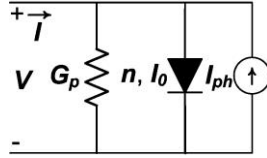Figure 33 presents the lumped parameter equivalent circuit model of a solar cell with series resistance and parallel conductance. The mathematical description of the terminal current of this equivalent circuit is given by the implicit equation:

$$I = I_0\left[\exp\left(\frac{V - I R_s}{n \, v_{th}}\right) - 1\right] + (V - I R_s) G_p - I_{ph} \quad . \tag{77}$$
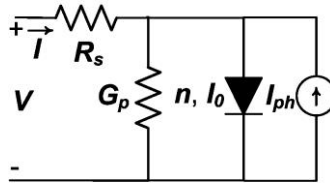

Fig. 33 Solar cell equivalent circuit with parasitic series and parallel resistances

The use of the special *Lambert W* function allows the above equation to be explicitly solved [54] for the terminal current as a function of the terminal voltage:

$$I = \frac{nv_{th}}{R_s} W_0 \left\{ \frac{I_0 R_s}{nv_{th}(1+R_s G_p)} \exp\left[\frac{V + R_s(I_0 + I_{ph})}{nv_{th}(1+R_s G_p)} \right] \right\} + \frac{VG_p - (I_0 + I_{ph})}{1+R_s G_p} \tag{78}$$

and for the terminal voltage as a function of the terminal current:

$$V = - nv_{th} W_0 \left[\frac{I_0}{nv_{th}G_p} \exp\left(\frac{I + I_0 + I_{ph}}{nv_{th}G_p} \right) \right] + I\left(R_s + \frac{1}{G_p} \right) + \frac{I_0 + I_{ph}}{G_p}. \tag{79}$$

An exact analytical solution for the maximum power point is not possible in this case either, because equating the derivative of the *V·I* product to zero does not allow to analytically solve for either V_{mpp} or I_{mpp}. Figure 34 illustrates the effect of series resistance and parallel conductance G_p on linear and semilogarithmic scale *I-V* characteristics simulated under illumination with different values of R_s and G_p.
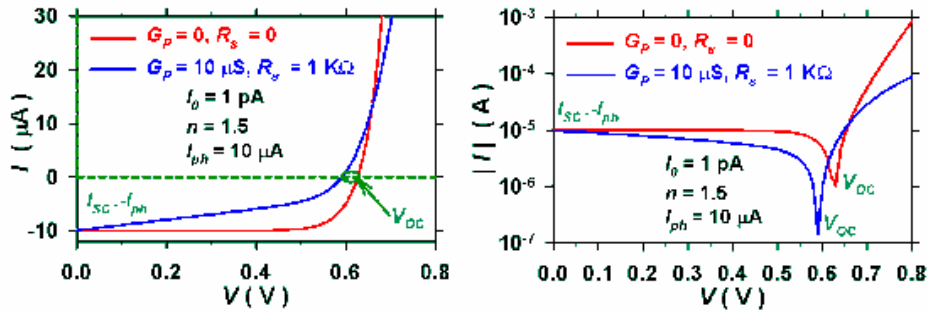
Fig. 34 Simulated *I-V* characteristic of a hypothetical solar cell with different values of series and parallel resistance in linear and logarithmic scales

The short circuit current is found by evaluating (78) at *V*=0, yielding:

$$I_{SC} = \frac{nv_{th}}{R_s} W_0 \left\{ \frac{I_0 R_s}{nv_{th}(1+R_s G_p)} \exp\left[\frac{R_s(I_0 + I_{ph})}{nv_{th}(1+R_s G_p)} \right] \right\} - \frac{(I_0 + I_{ph})}{1+R_s G_p} , \tag{80}$$

and the open circuit voltage V_{OC} is obtained by evaluating (79) at *I*=0, yielding:

$$V_{OC} = - nv_{th} W_0 \left[\frac{I_0}{nv_{th}G_P} \exp\left(\frac{I_0 + I_{ph}}{nv_{th}G_p} \right) \right] + \frac{I_0 + I_{ph}}{G_p}. \tag{81}$$

4.4.1. *Vertical optimization*

The implicit terminal current equation (77) could be directly fitted to the experimental data to extract the model parameters. However, a more convenient way [55], [56] would be to use instead the explicit equation (78) for the terminal current as a function of the

terminal voltage. Of course, this implies having a *Lambert W* function calculation añgorithm implemented within the data fitting software. Del Pozo et al [55] propose following this route by using MATLAB's non-linear curve fitting routine "*lsqcurvefit.*" This vertical optimization procedure (minimizing the current quadratic error) allows the extraction of all the parameters at the same time, but it frequently requires using good initial estimates of the parameters.

4.4.2. *Extraction from the Co-Content function*

Model parameters can be extracted from the integrals of the illuminated *I-V* characteristics. The integral with respect to the voltage is known as the Co-Content $CC(I,V)$. For an illuminated solar cell it is defined as [23], [24]:

$$CC(I,V) \equiv \int_0^V (I - I_{SC})\, dV \quad .\tag{82}$$

The lower limit of integration in the above equation is defined at the point $V=0$, $I=I_{sc}$. Substitution of (78) into (82) and integrating with respect to V results in a long expression that contains *Lambert W* functions and both variables V, and I. Replacing the terms that contain *Lambert W* functions of V, using equation (78), and after some algebraic manipulations, the function $CC(I,V)$ may be conveniently expressed for the solar cell as a purely algebraic equation of the form:

$$CC(I,V) = C_{V1}V + C_{I1}(I - I_{sc}) + C_{I1V1}V(I - I_{sc}) + C_{V2}V^2 + C_{I2}(I - I_{sc})^2 ,\tag{83}$$

where the five coefficients are given in terms of the model parameters by:

$$C_{I1} = R_s(I_0 + I_{ph} + I_{SC}) + nV_{th}(1 + G_p R_s) + I_{SC}\, R_s^2\, G_p ,\tag{84}$$

$$C_{V1} = -(I_0 + I_{ph} + I_{SC}) - nv_{th}G_p - I_{SC}R_sG_p ,\tag{85}$$

$$C_{I2} = \frac{R_s(1 + G_p R_s)}{2} ,\tag{86}$$

$$C_{V2} = \frac{G_p}{2} ,\tag{87}$$

and the fifth is a coefficient that is dependent on the others:

$$C_{I1V1} = \frac{1 - \sqrt{1 + 16 C_{I2}\, C_{V2}}}{2} .\tag{88}$$

As can be realized from (88), there are actually only four independent coefficients, (84)-(87), and therefore only four unknowns may be extracted uniquely. However, all the model parameters may be extracted. The extraction procedure consists of performing bivariate fitting of algebraic equation (83) to the Co-Content function CC as numerically calculated from the experimental data using (82). This bivariate fitting process yields the values of the four equation coefficients C_{V1}, C_{I1}, C_{V2}, C_{I2}, which are then used to calculate the solar cell's model parameters G_p, R_s, I_{ph}, n and I_0 as follows. The value of the shunt loss is calculated directly from (87):

$$G_p = 2\ C_{V2}\ . \tag{89}$$

The value of the series resistance is calculated by substituting (89) into (86) and solving the resulting quadratic equation:

$$R_s = \frac{\sqrt{1 + 16\ C_{V2}\ C_{I2}}\ - 1}{4\ C_{V2}}\ . \tag{90}$$

The value of the junction quality factor is calculated by substituting (89) and (90) into (84) and (85) and solving the two equations to yield:

$$n = \frac{C_{V1}\ (\sqrt{1+16\ C_{V2}\ C_{I2}}\ -\ 1)\ +\ 4\,C_{I1}\ C_{V2}}{4\ v_{th}\ C_{V2}}\ . \tag{91}$$

The value of the photo-generated current is obtained assuming $I_0 \ll I_{ph}$ as:

$$I_{ph} = -\frac{(1 + \sqrt{1 + 16\ C_{V2}\ C_{I2}})(C_{V1} + I_{SC})}{2}\ - 2\,C_{I1}C_{V2}\ . \tag{92}$$

And finally the value of I_0 is obtained by back substitution into (77) using the above extracted parameters:

$$I_0 = \frac{I - (V - I\,R_s)\,G_p + I_{ph}}{\exp\left(\dfrac{V\ -\ I\,R_s}{n\,v_{th}}\right) - 1}\ . \tag{93}$$

We will illustrate this parameter extraction method by applying it to published *I-V* characteristics of an illuminated experimental plastic solar cell [57]. Figure 35 shows the measured data together with the simulation play-back resulting from the use of the parameters extracted as described above. It must be pointed out that in order to obtain reasonably accurate results, it is advisable to use for measurement an small voltage step (at least 10 mV). Additionally, it is of paramount importance to use for numerical calculation a suitable integration algorithm, that is, one that will generate insignificant error, such as a closed Newton-Cotes formula with 7 points, as illustrated in the Appendix in [41].
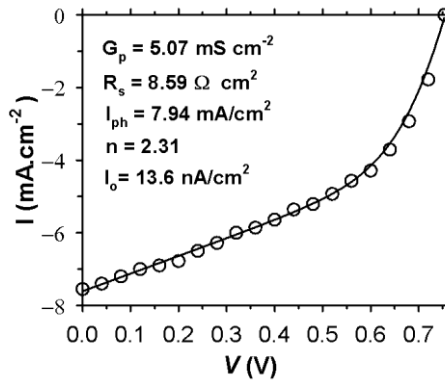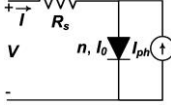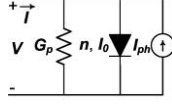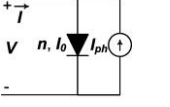

Fig. 35 Simulated single-exponential illuminated solar cell *I-V* characteristics (line) over the original experimental data points (symbols)

In order to facilitate the application of this method we present in Table 2 four coefficients of equation (83) and four model parameters for three representative cases.

Table 2 Three particular cases of a solar cell single-exponential model

	Case 1	Case 2	Case 3
C_{V1}	$-(I_0 + I_{ph} + I_{SC})$	$-(I_0 + I_{ph} + I_{SC}) - nv_{th}G_p$	$-(I_0 + I_{ph} + I_{SC})$
C_{I1}	$R_s(I_0 + I_{ph} + I_{SC}) + nv_{th}$	nv_{th}	nv_{th}
C_{V2}	0	$G_P/2$	0
C_{I2}	$R_s/2$	0	0
G_p	0	$2\,C_{V2}$	0
R_s	$2C_{I2}$	0	0
I_{ph}	$-(C_{V1} + I_{SC})$	$-C_{V1} - nv_{th}G_p + I_{SC}$	$-(C_{V1} + I_{SC})$
n	$[C_{I1} - R_s(I_{ph} + I_{SC})]/v_{th}$	C_{I1}/v_{th}	C_{I1}/v_{th}

4.4.3. *Extraction from the Content function*

Model parameters also can be extracted from the integral of voltage with respect to the current, using the Content instead of the Co-content. According to Peng et al [58] the Content is:

$$C(I,V) \equiv \int_0^I V\, dI = \frac{1}{2A}\left[(-V - BI + C)^2 - (-V + C)^2 \right] - \frac{BI^2}{2} + ADI . \qquad (94)$$

where

$$A = \frac{1}{G_p}, \qquad (95)$$

$$B = R_s + \frac{1}{G_p} \qquad (96)$$

$$C = nv_{th} + \frac{I_{ph} + I_0}{G_p}, \qquad (97)$$

and

$$D = I_{ph} + I_0. \qquad (98)$$

Once the coefficients A, B, C, and D are obtained from numerical bivariate fitting of (94), the model parameters G_p, R_s, I_{ph} and n are calculated from the above equations (with the assumption $I_0 \ll I_{ph}$) as follows:

$$G_p = \frac{1}{A} , \qquad (99)$$

$$R_s = \mathrm{B} - \mathrm{A}, \tag{100}$$

$$I_{ph} \approx \mathrm{D}, \tag{101}$$

and

$$n = \frac{(\mathrm{C} - \mathrm{AD})}{v_{th}}. \tag{102}$$

To numerically evaluate the integral that defines the Content, this procedure would normally require a set of voltage data corresponding to uniform step incrementing current data. Alternatively, the Content function could also be calculated using the fundamental relation between Content and Co-content: *C=IV-CC*.

4.4.4. *Sandia's sequential approach*

Hansen et al [59], [60], from Sandia National Laboratories, developed the following sequential approach to extract the model parameters of solar cells: a) The diode ideality factor n is obtained from the relationship between V_{OC} and effective irradiance. An alternative possibility for extracting n is to use the dark *I-V* characteristics. b) The parallel conductance G_p is obtained using the the Co-content function extraction method [24]. They propose to evaluate the *CC* function by first applying a spline interpolation method to the measured data and then use a trapezoidal numerical integration. c) I_0 is estimated using the open circuit condition ($V = V_{OC}$ and I=0) and the approximation $I_{ph} \cong -I_{SC}$:

$$I_0 = (-I_{SC} - G_P V_{OC}) \exp\left(\frac{-V_{OC}}{n v_{th}}\right). \tag{103}$$

d) I_{ph} is determined at short circuit conditions ($V = 0$ and $I=I_{SC}$):

$$I_{ph} = -I_{SC} + I_0 \left[\exp\left(\frac{-I_{SC} R_s}{n v_{th}}\right) - 1 \right] - I_{SC} R_s G_p. \tag{104}$$

4.4.5. *Approximate lateral optimization*

Chegaar et al [61] proposed an approximate function $F(I)$ to extract the parameters R_s, I_{ph}, I_0 and n:

$$F(I) = R_S I + n v_{th} \ln\left(1 + \frac{I + I_{ph}}{I_0}\right). \tag{105}$$

Thereafter the parallel conductance G_p is estimated from the commonly used approximation:

$$G_p \approx \frac{dI}{dV}\bigg|_{I=I_{SC}}. \tag{106}$$

This approximate function $F(I)$ is the rigorous voltage solution of the case of a single-exponential model with series resistance and G_p=0, represented by equation (69) in Section 4.2. Therefore, in essence this method is just an approximate lateral optimization, since $F(I) \approx V$.

4.4.6. *Regional optimization*

Bouzidi et al [62] proposed the use of two different equations to fit low and high voltage regions of the *I-V* characteristics. The linear part of the implicit equation (77) dominates for low voltage, and thus the following approximation is proposed:

$$I = (V - I R_s) G_P - I_{ph} \; . \tag{107}$$

Then, solving the above equation for the current, an approximate expression for low voltage is obtained:

$$I = \frac{V G_p - I_{ph}}{1 + R_s G_p} \; . \tag{108}$$

The exponential part dominates at high voltage, and the implicit equation can be approximated by neglecting the linear term in *V*:

$$I = I_0 \left[\exp\left(\frac{V - I R_s}{n \, v_{th}}\right) - 1 \right] - G_p R_s I - I_{ph} \; . \tag{109}$$

Finally, solving for the voltage in the above equation, the high voltage approximation is obtained:

$$V = I R_s + n \, v_{th} \ln\left[\frac{I(1 + G_p R_s) + I_{ph}}{I_0} + 1\right] \; . \tag{110}$$

4.4.7. *Lateral and vertical optimization*

Haouari-Merbah et al [63] propose using different fitting criteria for the low and high voltage ranges. A vertical optimization procedure (minimizing the current quadratic error) is to be used near short circuit, whereas a lateral optimization procedure (minimizing the voltage quadratic error) needs to be used near open circuit. Although the use of two different fitting criteria could improve extracted parameter accuracy, it certainly involves more complex numerical algorithms.

5. MULTIPLE-EXPONENTIAL SOLAR CELL MODEL

As in the case of other diodes, a single-exponential equation is frequently not enough to model many types of real solar cells, because it cannot adequately represent the several conduction phenomena that significantly contribute to the total current of the junction [18], [64]-[66].

5.1. Alternative multi-exponential model for solar cells with resistances

Figure 36 presents the lumped parameter equivalent circuit model of a solar cell that consists of various exponential-type ideal diodes, a photogenerated current source, a series parasitic resistance R_s, and two parallel parasitic conductances G_{p1} and G_{p2} . Its mathematical description is given by the implicit equation:

$$I = \sum_{k=1}^{N} I_{0k} \left[\exp\left(\frac{V - R_s(I - G_{p2}V)}{n \, v_{th}}\right) - 1 \right] - I_{ph} + G_{p2}V(1 + G_{p1}R_s) + G_{p1}(V - R_sI) \; . \tag{111}$$

In order to use Thevenin's theorem for solar cells in a rigorous way, we proceed first to separate the linear and nonlinear terms, as indicated in Fig. 36. The Thevenin equivalent circuit of the linear part defined in Fig. 37 is given by the Thevenin equivalent voltage V_{THE}, which includes the photogenerated current I_{ph}, and the Thevenin equivalent resistance R_{THE}, which only contains R_s and G_{p1}:

$$R_{THE} = \frac{R_s}{1 + G_{p1}R_s} \quad , \tag{112}$$

$$V_{THE} = \left(\frac{V}{R_s} + I_{ph} \right) R_{THE} \quad . \tag{113}$$
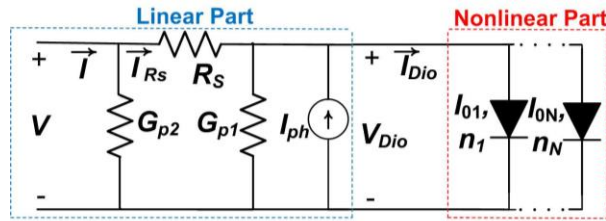

Fig. 36 Generic solar cell equivalent circuit including multiple diodes, parasitic series resistance, and two parallel conductances. For convenience, the linear and the nonlinear parts are separated by dashed boxes
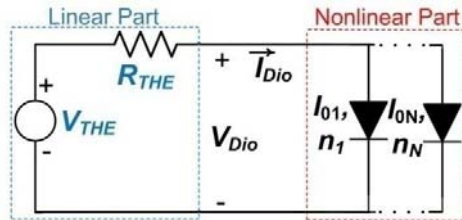

Fig. 37 Thevenin equivalent circuit used to obtain the voltage and the total current in the nonlinear part

Note that the absence of G_{p2} from the Thevenin equivalent resistance is correct, since it is perfectly congruent with the fact that I_{Dio} does not depend on G_{p2}. The effect of G_{p2} on the total current will be accounted for once I_{Dio} is calculated.

For a general case of N diodes in parallel, the total current in the nonlinear part, I_{Dio}, will be obtained numerically by using the circuit in Fig. 37. This procedure is equivalent to solving (111). The importance of the Thevenin equivalent circuit in Fig. 37 will be clarified when the approximation is presented.

To explain how to evaluate the variables that the Thevenin equivalent circuit has apparently concealed, we notice that once the total current flowing into the parallel combination of all diodes, I_{Dio}, is known, the voltage across the nonlinear part, V_{Dio}, can be expressed by writing:

$$V_{Dio} = V_{THE} - I_{Dio}\, R_{THE}\,. \tag{114}$$

Then, once the values of I_{Dio} and V_{Dio} are found, the total current is obtained by going back to the circuit shown in Fig. 36:

$$I = G_{p2}\, V + G_{p1}\, V_{Dio} - I_{ph} + I_{Dio}\,. \tag{115}$$

We have proposed [65] an explicit model as an alternative to the above discussed conventional implicit model depicted by the circuit shown in Fig. 36 and mathematically described by (111). It is represented by the circuit shown in Fig. 38.
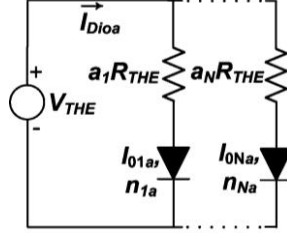

Fig. 38 The alternative model's equivalent circuit with multiple diodes and the Thevenin equivalent resistance in series with each diode

This model's *I–V* characteristics may be found by solving each branch separately and then adding their solutions together. Accordingly, the following explicit equation may be written for the total current into the diodes:

$$I = I_{Dioa} = \sum_{k=1}^{N} \left\{ \frac{n_{ka} v_{th}}{a_k R_{THE}} W_0 \left[\frac{a_k R_{THE} I_{0k}}{n_{ka} V_{th}} \exp\left(\frac{V_{THE} + a_k R_{THE} I_{0k}}{n_{ka} v_{th}} \right) \right] - I_{0k} \right\}\,, \tag{116}$$

where the single global series resistance, R_{THE}, present in the conventional model, has been replaced in this alternative model by individual resistances, $a_k R_{THE}$, placed in series at each of the *N* parallel current paths representing the different conduction mechanisms to be modeled.

Finally the total current is obtained by substituting (116) into (115) in combination with (112)-(114):

$$I = \sum_{k=1}^{N} \left\{ \frac{n_{ka} v_{th}}{a_k R_s} W_0 \left[\frac{a_k R_s I_{0k}}{n_{ka} v_{th}(1 + R_s G_{p1})} \exp\left(\frac{V + I_{ph} R_s + a_k R_s I_{0k}}{n_{ka} v_{th}(1 + R_s G_{p1})} \right) \right] - \frac{I_{0k}}{(1 + R_s G_{p1})} \right\}$$
$$+ \frac{V(G_{p1} + G_{p2} + G_{p1} G_{p2} R_s) - I_{ph}}{1 + R_s G_{p1}}\,. \tag{117}$$

Figure 39 presents original synthetic data generated by the conventional double-exponential implicit model corresponding to a ZnO/CdS/CuGaSe$_2$ solar cell presented by Saad and A. Kassis [64], together with the alternative model playback produced by the explicit double-exponential equation using the extracted parameters indicated in Table 3. The excellent correspondence between both models attests to the suitability of the alternative explicit equation to faithfully reproduce the *I-V* characteristics of typical junction solar cells.
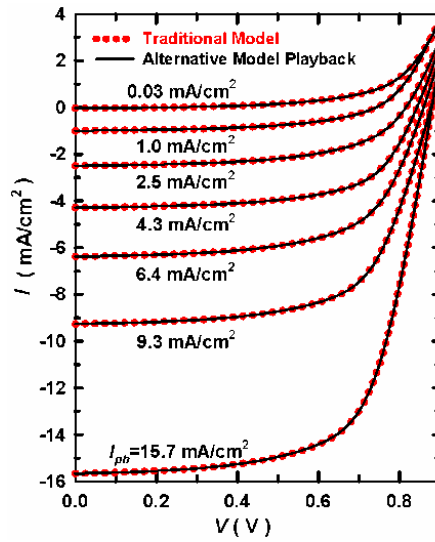
Fig. 39 Synthetic illuminated *I–V* characteristics (red symbols) corresponding to a ZnO/CdS/CuGaSe$_2$ solar cell from [64] simulated using the traditional model and the alternative model's playback (black solid lines)

Table 3 Comparison of original and extracted alternative parameters of the solar cell presented by Saad and Kassis [64] for various illumination levels

Extracted Model Parameters		Illumination level (in terms of I_{ph} [mA.cm^{-2}])			
		15.7	9.3	6.4	4.3
Conventional model	**Alternative model**				
I_{01} [A.cm^{-2}]	I_{01a} [A.cm^{-2}]	1.5 x10^{-5}	9.8 x10^{-6}	8.1 x10^{-6}	7.1 x10^{-6}
		1.9 x10^{-5}	1.2x10^{-5}	9.5x10^{-6}	7.9x10^{-6}
I_{02} [A.cm^{-2}]	I_{02a} [A.cm^{-2}]	1.6 x10^{-14}	9.3 x10^{-16}	1.1x10^{-15}	6.7 x10^{-16}
		3.6x10^{-15}	1.4x10^{-16}	1.2x10^{-16}	1.1x10^{-16}
n_1	n_{1a}	6.54	6.44	6.24	6.42
		7.16	7.00	6.55	6.66
n_2	n_{2a}	1.37	1.27	1.28	1.24
		1.27	1.16	1.15	1.14
R_{TH} [Ω.cm^2]	a_1R_{TH} [Ωcm^2]	25.68	33.94	25.55	27.58
		7.00	12.17	13.27	15.07
	a_2R_{TH} [Ωcm^2]	8.08	14.74	17.11	18.72
G_{p1} [mS.cm^{-2}]		0.2	0.204	0.189	0.152
R_s [Ω.cm^2]		7.01	12.20	13.30	15.10

5.2. Approximate lateral optimization

Figure 40 presents the lumped parameter equivalent circuit model of a solar cell that consists of various exponential-type ideal diodes, a photogenerated current source, and only a parasitic series resistance R_s. Its mathematical description is given by the implicit equation

$$I = \left\{ \sum_{k=1}^{N} I_{0k} \left[\exp\left(\frac{V - R_s I}{n \, v_{th}} \right) - 1 \right] \right\} - I_{ph} \quad . \tag{118}$$
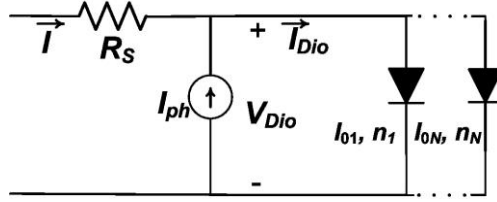

Fig. 40 Multi-exponential solar cell equivalent circuit including only a parasitic series resistance

Unfortunately, neither the terminal current nor the terminal voltage are solvable as exact explicit functions of each other for arbitrary values of "ideality" factors, n_k. There are two notable exceptions that allow (118) to be explicitly and exactly solved for the terminal variables: a) when $N=1$, which corresponds to the case of the simple single exponential model, whose explicit solutions for both the current and voltage are well known even in the presence of significant parasitic series and shunt resistances [24], [54], and b) when $N=2$ and the values of the ideality factors are known to be one equal to twice the other ($n_2=2n_1$), which corresponds to the case of the quite common double-exponential model already discussed for common diodes. In this second case the defining equation (118) takes on a quadratic form and thus the solution for the terminal voltage is exactly given by [49], [65]:

$$V = R_s I + 2 n_1 v_{th} \ln \left[\sqrt{ \left(\frac{I_{02}}{2 I_{01}} + 1 \right)^2 + \frac{I + I_{ph}}{I_{01}} } - \frac{I_{02}}{2 I_{01}} \right] \quad . \tag{119}$$

Notice that by letting $I_{02}=0$ in (119) the above solution readily reduces to that of the well known single exponential ($N=1$) case:

$$V = R_s I + n_1 v_{th} \ln \left(\frac{I + I_{ph}}{I_{01}} + 1 \right) \quad . \tag{120}$$

This combination of ideality factors $n_2=2n_1$, with $n_1=1$, corresponds the double-exponential model that is most widely encountered in the literature, since these two values of n ideally characterize the drift-diffusion and recombination conduction mechanisms dominant in ordinary mono-crystalline homo-junctions.

Although the terminal voltage may be expressed as an exact explicit function of the terminal current when of $N=2$ and $n_2=2n_1$, as (119) reveals, the opposite is not true, because the single lumped parasitic series resistance present prevents the terminal current from being expressed exactly as an explicit function of the terminal voltage.

The proposed approximate solution of transcendental equation (118) for the terminal voltage as an explicit function of the terminal current valid for arbitrary N, I_{0k}, and n_k is:

$$V \approx R_S\, I - m\, v_{th}\, \ln\left[\sum_{k=1}^{N} \left(\frac{I+I_{ph}}{I_{0k}} +1 \right)^{-\frac{n_k}{m}} \right], \tag{121}$$

where m represents an empiric dimensionless joining factor. It is important to note in (121) that, at a any particular bias point (I,V) at which only one of the conduction mechanisms represented by one of the diodes in the model is dominant, the summation in the above equation reduces to just one term, and thus (121) approaches (120) at that bias point (I,V). For the specific case of a model with two parallel diodes ($N=2$) with arbitrary values of n_1 and n_2, the approximate terminal voltage solution simplifies to:

$$V \approx R_S\, I - m\, v_{th}\, \ln\left[\left(\frac{I+I_{ph}}{I_{01}} +1 \right)^{-\frac{n_1}{m}} + \left(\frac{I+I_{ph}}{I_{02}} +1 \right)^{-\frac{n_2}{m}} \right]. \tag{122}$$

To validate the applicability of the presently proposed approximate solution of the terminal voltage, we tested (122) on a ZnO/CdS/CuGaSe$_2$ solar cell's synthetic characteristics obtained using a double-exponential model with parameters as reported in [64]: $J_{ph}=15.7$ mA.cm^{-2}, $n_1=1.27$, $n_2=7.16$, $J_{01}=3.6\times10^{-15}$ A cm^{-2}, $J_{02}=1.91\times10^{-5}$ A cm^{-2}, and $R_S=7\ \Omega$ cm^2.

Figure 41 shows the synthetic I-V characteristics calculated using the traditional model together with those calculated using the present approximate model, as defined by equation (122) with the extracted parameters. Using a joining factor of $m=2.65$, the extracted parameters were: $J_{ph}=15.7$ mA.cm^{-2}, $n_1=1.43$, $n_2=7.45$, $J_{01}=1.24\times10^{-13}$ A cm^{-2}, $J_{02}=2.13\times10^{-5}$ A cm^{-2}, and $R_S=6.99\ \Omega$ cm^2. The corresponding absolute lateral error is also included in the figure. The joining factor was slightly adjusted to $m=2.6$ in order to produce the best smoothing possible at the transition region. We observe that the resulting maximum absolute lateral error is less than 4 mV. A logarithmic plot of $(J + J_{ph})$ better illustrates the presence of the two dominant conduction mechanisms, as evidenced by the easily observable double slope shown in the same Fig. 41.
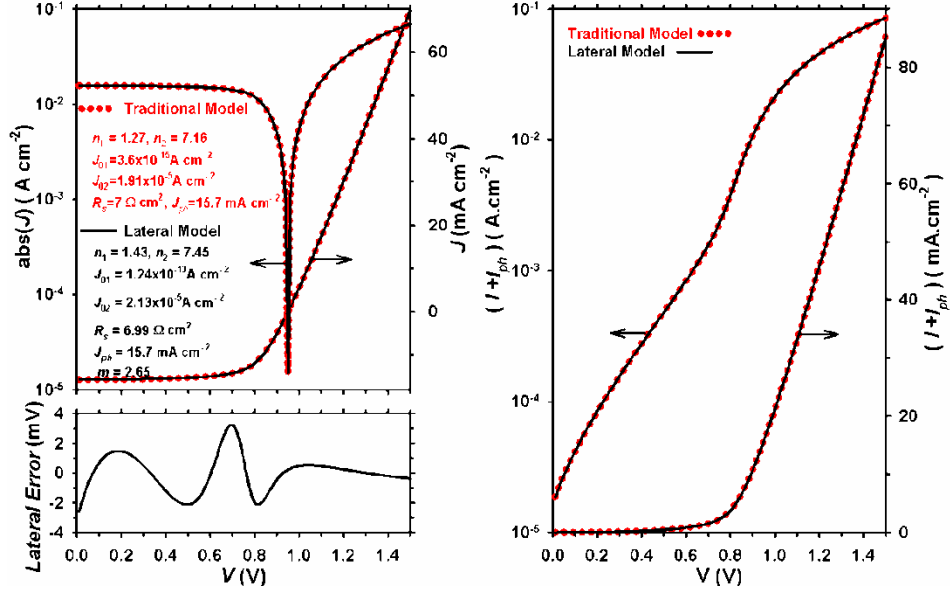
Fig. 41 (Left upper pane) Illuminated *J-V* characteristics playbacks calculated using traditional (red dotted lines) and proposed lateral (black solid lines) models of a solar cell in linear and logarithmic scales. (Left lower pane) resulting lateral error of proposed model. (Right pane) Playback of the shifted current density-voltage characteristics $(J+J_{ph})$-*V* under illumination, calculated using the traditional (red dotted lines) and the proposed lateral (black solid lines) models of a ZnO/CdS/CuGaSe$_2$ solar cell in linear and logarithmic scales using the same parameters indicated in the left upper pane

6. CONCLUSIONS

We have presented, reviewed and critically compared the foremost methods most commonly used for parameter value extraction in lumped parameter equivalent circuit diode and solar cell models. The comparisons were done by classifying these methods according to their corresponding lumped parameter equivalent circuit models. We have emphasized throughout the paper that the best method for any particular application depends very much on the appropriateness of the lumped parameter equivalent circuit used to model the cell. We have recommend the use of methods based on many data points, using for example numerical integration or optimization, as a means to reduce the extraction uncertainties arising from the probable presence of noise in the measured data.

REFERENCES

[1] P.J. Chen, S.C. Pao, A. Neugroschel, F.A. Lindholm, "Experimental determination of series resistance of p-n junction diodes and solar cells", IEEE Transactions on Electron Devices, vol. ED-25, pp. 386-388, March 1978. http://dx.doi.org/10.1109/T-ED.1978.19089

[2] D.T. Cotfas, P.A. Cotfas, S. Kaplanis, "Methods to determine the dc parameters of solar cells: A critical review", Renewable and Sustainable Energy Reviews, vol. 28, pp. 588-596, Dec. 2013. http://dx.doi.org/10.1016/j.rser.2013.08.017

[3] D.T. Cotfas, P.A. Cotfas, D. Ursutiu, C. Samoila, , "The methods to determine the series resistance and the ideality factor of diode for solar cells-review", In Proceedings of the 13th Int. Conf. Optimization of Electrical and Electronic Equipment (OPTIM), Brasov, Romania, 2012, pp. 966-972. http://dx.doi.org/10.1109/OPTIM.2012.6231814

[4] Li, Y., Huang, W., Huang, H., Hewitt, C., Chen, Y., Fang, G., Carroll, D.L., "Evaluation of methods to extract parameters from current-voltage characteristics of solar cells", Solar Energy, vol. 90, pp. 51-57, April 2013. http://dx.doi.org/10.1016/j.solener.2012.12.005

[5] D. Pysch, A. Mette, S.W. Glunz, , "A review and comparison of different methods to determine the series resistance of solar cells", Solar Energy Materials and Solar Cells, vol. 91, pp. 1698-1706, Nov. 2007. http://dx.doi.org/10.1016/j.solmat.2007.05.026

[6] M. Bashahu, P. Nkundabakura, "Review and tests of methods for the determination of the solar cell junction ideality factors", Solar Energy, vol. 81, pp. 856-863, July 2007. http://dx.doi.org/10.1016/j.solener.2006.11.002

[7] M. Sabry, A.E. Ghitas, , "Influence of temperature on methods for determining silicon solar cell series resistance", Journal of Solar Energy Engineering, Transactions of the ASME, vol. 129, pp. 331-335, Jan. 2007. http://dx.doi.org/10.1115/1.2735350

[8] M. Chegaar, Z. Ouennoughi, F. Guechi, , "Extracting dc parameters of solar cells under illumination", Vacuum, vol. 75, pp. 367-372, Aug. 2004. http://dx.doi.org/10.1016/j.vacuum.2004.05.001

[9] M. Bashahu, A. Habyarimana, "Review and test of methods for determination of the solar cell series resistance", Renewable Energy, vol. 6, pp. 129-138, March 1995. http://dx.doi.org/10.1016/0960-1481(94)E0021-V

[10] P. Mialhe, A. Khoury, J.P. Charles, "Review of techniques to determine the series resistance of solar cells", Physica Status Solidi (A) Applied Research, vol. 83, Issue 1, pp. 403-409 , May 1984. http://dx.doi.org/10.1002/pssa.2210830146

[11] P. Mialhe, J.P. Charles, A. Khoury, G. Bordure, "The diode quality factor of solar cells under illumination", Journal of Physics D: Applied Physics, vol. 19, art. no. 018 , pp. 483-492, 1986. http://dx.doi.org/10.1088/0022-3727/19/3/018

[12] R. S. Ohl, "Light-sensitive electric device", U.S. Patent 2402662. Filed May 27, 1941, Issue: Jun 25, 1946. http://www.archpatent.com/patents/2402662

[13] G.L. Pearson, W.H. Brattain, "History of Semiconductor Research", Proceedings of the IRE, vol 43, pp. 1794-1806, Dec. 1955. http://dx.doi.org/10.1109/JRPROC.1955.278042

[14] M. Riordan, L. Hoddeson, , "Origins of the pn junction", IEEE Spectrum, vol. 34, pp. 46-51, June 1997. http://dx.doi.org/10.1109/6.591664

[15] W. Shockley, "The theory of p-n junctions in semiconductors and p-n junction transistors", Bell Syst. Tech. J., vol. 28, pp. 435-489, July 1949. Available at: http://www.alcatel-lucent.com/bstj/vol28-1949/bstj-vol28-issue03.html

[16] D. M. Chapin, C. S. Fuller, and G. L. Pearson, "A New Silicon pn Junction Photocell for Converting Solar Radiation into Electrical Power", J. Appl. Phys., vol. 25, 676-677, 1954. http://dx.doi.org/10.1063/1.1721711

[17] M. B. Prince, "Silicon Solar Energy Converters", J. Appl. Phys., vol. 26, 534-540, May 1955. http://dx.doi.org/10.1063/1.1722034

[18] C.T. Sah, R.N. Noyce, W. Shockley, "Carrier generation and recombination in P-N junctions and P-N junction characteristics", Proc IRE; vol. 45, pp. 1228–1243, Sept. 1957. http://dx.doi.org/10.1109/JRPROC.1957.278528

[19] D.S.H. Chan, J.R. Phillips, J.C.H. Phang, "A comparative study of extraction methods for solar cell model parameters", Solid-State Electronics, vol. 29, 329–337, March 1986. http://dx.doi.org/10.1016/0038-1101(86)90212-1

[20] S. Lineykin, M. Averbukh, A. Kuperman, "An improved approach to extract the single-diode equivalent circuit parameters of a photovoltaic cell/panel", Renewable and Sustainable Energy Reviews, vol. 30 , pp. 282-289, Feb. 2014. http://dx.doi.org/10.1016/j.rser.2013.10.015

[21] L. Peng, Y. Sun, Z. Meng, "An improved model and parameters extraction for photovoltaic cells using only three state points at standard test condition", Journal of Power Sources, vol. 248, pp. 621-631, Feb. 2014. http://dx.doi.org/10.1016/j.jpowsour.2013.07.058

[22] F.J. García-Sánchez, A.Ortiz-Conde, G. De Mercato, J.J. Liou, L. Recht, "Eliminating parasitic resistances in parameter extraction of semiconductor device models", In Proceedings of the 1st IEEE ICCDCS, Caracas, Venezuela, 1995, pp. 298-302. http://dx.doi.org/10.1109/ICCDCS.1995.499164

[23] F.J. García Sánchez, A. Ortiz-Conde, and J.J. Liou, "A parasitic series resistance-independent method for device-model parameter extraction", IEE Proc. Cir. Dev. and Sys., vol. 143, pp. 68-70, Feb. 1996. http://dx.doi.org/10.1049/ip-cds:19960159

[24] A. Ortiz-Conde, F. J. García Sánchez , and J. Muci, "New method to extract the model parameters of solar cells from the explicit analytic solutions of their illuminated I-V characteristics", Solar Energy Materials and Solar Cells, vol. 90, pp. 352–361, Feb. 2006. http://dx.doi.org/10.1016/j.solmat.2005.04.023

[25] A. Ortiz-Conde et al "Direct extraction of semiconductor device parameters using lateral optimization method", Solid-State Electronics, vol. 43, pp. 845-848, April 1999. http://dx.doi.org/10.1016/S0038-1101(99)00044-1

[26] J. Appelbaum, A. Peled, "Parameters extraction of solar cells – A comparative examination of three methods", Solar Energy Materials and Solar Cells, vol. 122, pp. 164-173, March 2014. http://dx.doi.org/10.1016/j.solmat.2013.11.011

[27] N. Moldovan, R. Picos, E. Garcia-Moreno, "Parameter extraction of a solar cell, compact model using genetic algorithms", In Proceedings of the Spanish Conf Electron Dev (CDE'09), Santiago de Compostela, Spain, 2009, pp. 379–82. http://dx.doi.org/10.1109/SCED.2009.4800512

[28] Hachana, O., Hemsas, K.E., Tina, G.M., Ventura, C., "Comparison of different metaheuristic algorithms for parameter identification of photovoltaic cell/module", Journal of Renewable and Sustainable Energy 5 (5) , art. no. 053122, Sept. 2013. http://dx.doi.org/10.1063/1.4822054

[29] T.C. Banwell and A. Jayakumar, "Exact analytical solution for current flow through diode with series resistance", Electronics Letters, vol. 36, pp. 291-292, Feb. 2000. http://dx.doi.org/10.1049/el:20000301

[30] T.C. Banwell, "Bipolar transistor circuit analysis using the Lambert W-function", IEEE Transactions on Circuits and Systems I: Fundamental Theory and Applications vol. 47 (11), pp. 1621-1633, Nov. 2000. http://dx.doi.org/10.1109/81.895330

[31] R.M. Corless, G.H. Gonnet, D.E.G. Hare, D.J. Jeffrey, D.E. Knuth, "On the Lambert W function", Advances in Computational Mathematics, vol. 5, pp. 329-359, Dec. 1996. http://dx.doi.org/10.1007/BF02124750

[32] S.R. Valluri, D.J. Jeffrey, R.M. Corless, "Some applications of the Lambert W function to physics". Can. J. Phys, vol. 78, pp. 823–831, Sept. 2000. http://dx.doi.org/10.1139/p00-065

[33] A. Ortiz-Conde, F. J. García Sánchez and M. Guzmán, " Exact analytical solution of channel surface potential as an explicit function of gate voltage in undoped-body MOSFETs using the lambert w function and a threshold voltage definition therefrom", Solid-State Electronics, vol.47, pp. 2067-2074, Nov. 2003. http://dx.doi.org/10.1016/S0038-1101(99)00044-1

[34] K. Lee, M. Shur, T.A. Fjeldly, T. Ytterdal, Semiconductor Device Modeling for VLSI. Englewood Cliffs: Prentice-Hall, 1993. See also: AIM-SPICE, http://www.aimspice.com .

[35] R.J. Bennett, "Interpretation of forward bias behavior of schottky barriers", IEEE Transactions on Electron Devices, vol. ED-34, pp. 935-937, April 1987. http://dx.doi.org/10.1109/T-ED.1987.23020

[36] G. L. Araujo and E. Sanchez, "New method for experimental determination of the series resistance of a solar cell", IEEE Transactions on Electron Devices, vol. ED-29, pp. 1511-1513, Oct. 1982. http://dx.doi.org/10.1109/T-ED.1982.20906

[37] A. Ortiz-Conde, F.J. García Sánchez, P.E. Schmidt, and R.J. Laurence, Jr., "Extraction of diode parameters from the integration of the forward current", In Proceedings of the Second International Semiconductor Device Research Symposium, Charlottesville, Virginia, 1993, vol. 2, pp. 531-534.

[38] A. Ortiz-Conde, F.J. García Sánchez, J.J. Liou, J. Andrian, R.J. Laurence, and P.E. Schmidt, "A generalized model for a two-terminal device and its application to parameters extraction", Solid-State Electronics, vol. 38, pp. 265-266, Jan. 1995. http://dx.doi.org/10.1016/0038-1101(94)00141-2

[39] A. Kaminski, J.J. Marchand, A. Fave, A. Laugier, "New method of parameters extraction from dark I-V curve", In Proceedings of the Twenty-Sixth IEEE Photovoltaic Specialists Conf., Anaheim, CA, 1997, pp. 203-206. http://dx.doi.org/10.1109/PVSC.1997.654064

[40] A. Cerdeira, M. Estrada, R. Quintero, D. Flandre, A. Ortiz-Conde, F.J. García Sánchez, "New method for determination of harmonic distortion in SOI FD transistors", Solid-State Electronics, vol. 46, pp. 103-108, Jan. 2002. http://dx.doi.org/10.1016/S0038-1101(01)00258-1

[41] R. Salazar, A. Ortiz-Conde, F. J. García Sánchez, C.-S. Ho, and J.J. Liou, "Evaluating MOSFET Harmonic Distortion by Successive Integration of the I-V Characteristics", Solid-State Electronics, vol. 52, pp. 1092-1098, July 2008. http://dx.doi.org/10.1016/j.sse.2008.03.018

[42] H. Norde, "A modified forward I-V plot for Schottky diodes with high series resistance", Journal of Applied Physics, vol. 50, pp. 5052-5053, July 1979. http://dx.doi.org/10.1063/1.325607

[43] C. D. Lien, F.C.T. So, M.A. Nicolet, "An improved forward I-V method for nonideal Schottky diodes with high series resistance", IEEE Trans. Electron Dev., vol. 31, pp. 1502-1503, Oct. 1984. http://dx.doi.org/10.1109/T-ED.1984.21739

[44] K.E. Bohlin, , "Generalized Norde plot including determination of the ideality factor", J. Appl. Phys., vol. 60, p. 1223-1224, Aug. 1986. http://dx.doi.org/10.1063/1.337372

[45] S.K. Cheung, N.W. Cheung, "Extraction of Schottky diode parameters from forward current-voltage characteristics", Applied Physics Letters, vol. 49, pp. 85-87, July 1986. http://dx.doi.org/10.1063/1.97359

[46] A. Ortiz-Conde, F.J. García Sánchez, J. Muci, "Exact analytical solutions of the forward non-ideal diode equation with series and shunt parasitic resistances" Solid-State Electronics, vol. 44, pp. 1861-1864, Oct. 2000. http://dx.doi.org/10.1016/S0038-1101(00)00132-5

[47] A. Ortiz-Conde and F. J. García Sánchez, "Extraction of non-ideal junction model parameters from the explicit analytic solutions of its I–V characteristics", Solid-State Electronics, vol.49, pp. 465-472, March 2005. http://dx.doi.org/10.1016/j.sse.2004.12.001

[48] J.C. Ranuárez, A. Ortiz-Conde, F. J. García-Sánchez, "A new method to extract diode parameters under the presence of parasitic series and shunt resistance," Microelectronics Reliability, vol. 40, pp. 355-358 Feb. 2000. http://dx.doi.org/10.1016/S0026-2714(99)00232-2

[49] D.C. Lugo Muñoz, M. de Souza, M.A. Pavanello, D. Flandre. J. Muci, A. Ortiz-Conde, and F.J. García Sánchez, "Parameter Extraction in Quadratic Exponential Junction Model with Series Resistance using Global Lateral Fitting". In Proceedings of the 25th Symposium on Microelectronics Technology and Devices (SBMicro), São Paulo, Brasil, 2010. See also: Electrochemical Society Transactions, Vol. 31, pp. 369-376, 2010.   http://dx.doi.org/10.1149/1.3474181

[50] Yadir, S., Assal, S., El Rhassouli, A., Sidki, M., Benhmida, M., "A new technique for extracting physical parameters of a solar cell model from the double exponential model (DECM)", Optical Materials vol. 36, pp. 18-21, Nov. 2013. http://dx.doi.org/10.1016/j.optmat.2013.07.010

[51] J.C. Ranuárez, F. J. García Sánchez, and A. Ortiz-Conde, "Procedure for determining diode parameters at very low forward voltage," Solid-St. Electron., vol. 43, pp. 2129-2133, Dic. 1999. http://dx.doi.org/10.1016/S0038-1101(99)00181-1

[52] D.C. Lugo-Muñoz; J. Muci, A. Ortiz-Conde, F. J. García Sánchez , M. de Souza, M.A. Pavanello, "An explicit multi-exponential model for semiconductor junctions with series and shunt resistances", Microelectronics Reliability, vol. 51 pp. 2044–2048, Dec. 2011. http://dx.doi.org/10.1016/j.microrel.2011.06.030

[53] A. Ortiz-Conde, F.J. García Sánchez, A. Terán Barrios, J. Muci, M. de Souza, M.A. Pavanello "Approximate analytical expression for the terminal voltage in multi-exponential diode models", Solid-State Electronics, vol. 89, pp. 7-11, Nov. 2013. http://dx.doi.org/10.1016/j.sse.2013.06.010

[54] A. Jain, A. Kapoor, "Exact analytical solutions of the parameters of real solar cells using Lambert W-function", Solar Energy Materials and Solar Cells, vol. 81, pp. 269-277, Feb. 2004. http://dx.doi.org/10.1016/j.solmat.2003.11.018

[55] G. Del Pozo, B. Romero, B. Arredondo, , "Extraction of circuital parameters of organic solar cells using the exact solution based on Lambert W-function", In Proceedings of the International Society for Optical Engineering (SPIE), Brussels, Belgium 2012, art. no. 84351Z. http://dx.doi.org/10.1117/12.922461

[56] P. Hruska, Z. Chobola, L. Grmela, "Diode I-U curve fitting with Lambert W function", In Proceedings of the 25th International Conference on Microelectronics (MIEL), Belgrade, Yugoslavia, 2006, pp. 501-504. http://dx.doi.org/10.1109/ICMEL.2006.1651003

[57] Jeranko, H. Tributsch, N.S. Sariciftci, J.C. Hummelen, "Patterns of efficiency and degradation of composite polymer solar cells", Solar Energy Materials and Solar Cells, vol. 83, pp. 247-262, June 2004. http://dx.doi.org/10.1016/j.solmat.2004.02.028

[58] L. Peng, Y. Sun, Z. Meng, Y. Wang, Y. Xu, A new method for determining the characteristics of solar cells, Journal of Power Sources, vol. 227, pp. 131-136,   April 2013. http://dx.doi.org/10.1016/j.jpowsour.2012.07.061

[59] C.W. Hansen, A. Luketa-Hanlin, J.S. Stein, "Sensitivity of Single Diode Models for Photovoltaic Modules to Method Used for Parameter Estimation", In Proceedings of the 28th European PV Solar Energy Conf., Paris, France, pp. 3258-3264, 2013. http://dx.doi.org/10.4229/28thEUPVSEC2013-4AV.5.27

[60] C.W. Hansen, "Estimation of Parameters for Single Diode Models Using Measured IV Curves", Technical Report, Sandia National Laboratories, Albuquerque, NM, 2013. http://energy.sandia.gov/wp/wp-content/gallery/uploads/Hansen_SAND2013-4759C_PVSC391.pdf

[61] M. Chegaar, G. Azzouzi, P. Mialhe, , "Simple parameter extraction method for illuminated solar cells", Solid-State Electronics, vol. 50, pp. 1234-1237, July–Aug. 2006. http://dx.doi.org/10.1016/j.sse.2006.05.020

[62] K. Bouzidi, M. Chegaar, A. Bouhemadou, "Solar cells parameters evaluation considering the series and shunt resistance", Solar Energy Materials and Solar Cells, vol. 91, pp. 1647-1651, Nov. 2007. http://dx.doi.org/10.1016/j.solmat.2007.05.019

[63] M. Haouari-Merbah, M. Belhamel, I. Tobías, J.M. Ruiz, "Extraction and analysis of solar cell parameters from the illuminated current-voltage curve", Solar Energy Materials and Solar Cells, vol. 87, pp. 225-233, May 2005. http://dx.doi.org/10.1016/j.solmat.2004.07.019

[64] M. Saad and A. Kassis, "Current–voltage analysis of the record-efficiency CuGaSe2 solar cell: Application of the current separation method and the interface recombination model," Sol. Energy Mat. Sol. Cells, vol. 95, pp. 1927–1931, July 2011. http://dx.doi.org/10.1016/j.solmat.2011.02.022

[65] A. Ortiz-Conde, D. Lugo-Muñoz and F. J. García Sánchez, " An explicit multi-exponential model as an alternative to traditional solar cell models with series and shunt resistances", IEEE Journal of Photovoltaics, vol. 2, pp. 261-268, July 2012. http://dx.doi.org/10.1109/JPHOTOV.2012.2190265

[66] F.J. García Sánchez, Denise Lugo-Muñoz, J. Muci, and A. Ortiz-Conde, "Lumped Parameter Modeling of Organic Solar Cells' S-Shaped I–V Characteristics", IEEE Journal of Photovoltaics, vol. 3, pp. 330-335, Jan. 2013. http://dx.doi.org/10.1109/JPHOTOV.2012.2219503